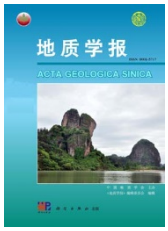

地质学报
Acta Geologica Sinica
ISSN 0001-5717,CN 11-1951/P

《地质学报》网络首发论文

题目：华南米仓山南缘中生代以来多阶段隆升-剥蚀过程与构造沉积耦合特征
作者：张梦霏，邱楠生，常健，冯乾乾，李晨星，刘鑫，龙康杰
DOI：10.19762/j.cnki.dizhixuebao.2025370
收稿日期：2025-09-11
网络首发日期：2026-01-15
引用格式：张梦霏，邱楠生，常健，冯乾乾，李晨星，刘鑫，龙康杰．华南米仓山南缘中生代以来多阶段隆升-剥蚀过程与构造沉积耦合特征[J/OL]．地质学报．https://doi.org/10.19762/j.cnki.dizhixuebao.2025370

华南米仓山南缘中生代以来多阶段隆升-剥蚀过程与构造沉积耦合特征

张梦霏[1,2)]，邱楠生*[1,2)]，常健*[1,2)]，冯乾乾[3)]，李晨星[1,2)]，刘鑫[1,2)]，龙康杰[1,2)]

1）中国石油大学(北京)油气资源与工程全国重点实验室，北京，102249；

2）中国石油大学(北京)地球科学学院，北京，102249；

3）中国石油大学(北京)碳中和示范性能源学院，北京，102249

内容提要：米仓山隆起的形成与板块碰撞和秦岭造山带的隆起关系密切，对其研究多聚焦在中-晚中生代以来的隆升-剥蚀过程，但对其初始隆升时间及隆升过程存在争议。本文选取米仓山南缘震旦系样品开展低温热年代学实验，并结合区域中生界碎屑锆石 U-Pb 年龄，系统重建了该区域早中生代以来的多阶段隆升-剥蚀过程。研究结果显示，锆石裂变径迹的中值年龄范围为 277±27～399±39 Ma，锆石(U-Th)/He 年龄范围为 136.4±6.8～290.0±14.5 Ma。通过热史模拟可将米仓山隆起自中生代以来的构造演化划分为 4 个阶段：① 晚三叠世到中侏罗世，受勉略洋闭合及扬子地块向秦岭地块俯冲影响，米仓山地区开始初始缓慢隆升；② 晚侏罗世到早白垩世，秦岭地块与扬子地块的持续碰撞引发强烈陆内造山，导致米仓山地区快速隆升；③ 晚白垩世到新中新世，受区域板块运动调整的影响，短暂进入构造停滞期；④ 中新世以来，受青藏高原隆升向东传递的影响，再次发生快速隆升剥蚀。碎屑锆石 U-Pb 年龄频谱分析表明四川盆地北部上三叠统到下侏罗统中新元古代的锆石明显增多，该现象揭示的米仓山地区在晚三叠世已经发生隆升，与低温热年代学数据所反映的初始隆升时间高度吻合。本研究恢复了米仓山南缘自中生代以来的构造-热演化史，明确了多阶段隆升-剥蚀过程与多幕次板块构造运动的时空耦合关系，为研究板块碰撞和秦岭造山带演化提供了新的证据。

关键词：米仓山；构造-热演化；低温热年代学；中生代；物源分析

低温热年代学定年体系主要通过分析样品的裂变径迹年龄与长度、(U-Th)/He 年龄等数据进行热历史模拟，进而定量揭示山体或沉积盆地经历的构造-热演化(田云涛等，2017；邱楠生等，2020)。该体系主要包括裂变径迹和(U-Th)/He 两种方法：前者是基于矿物内^{238}U 自发裂变产生裂变径迹，结合封闭温度和退火动力学原理，通过径迹年龄和长度分布反演矿物温度演化历史(Gleadow et al.，1986；李晨星等，2025)；而后者则依据矿物颗粒中 U、Th 衰变产生 He 在矿物中的累积与温度变化之间的关系，通过精准测量 U、Th、He 含量获取年龄，来限定热事件起始时限和温度变化速率，进而追踪区域热史演化(Wolf et al.，1996；邱楠生等，2010；Taylor and Fitzgerald，2011)。锆石和磷灰石是当前应用最成熟的低温热年代学定年矿物，其组合可约束 40～350℃温度区间的精细热演化，可有效研究深层、古老地质体的热历史和造山带复杂的隆升-剥蚀过程(Hendrix et al.，1994；Reiners et al.，2003；邱楠生等，2010；彭恒等，2018)。

盆地沉积物是源-汇系统的关键载体，记录了造山带的隆升信息(闫义等，2002；Lease et al.，2007；Li Yingqiang et al.，2016；Shao Tongbin et al.，2016；Wang Anqi et al.，2021)。其中碎屑锆石因抗风化能力强、U-Pb 同位素体系稳定，其年龄反

注：本文为国家自然科学基金项目(编号 U24B6001)资助的成果。
收稿日期：2025-09-11；改回日期：2025-11-27；责任编辑：蔡志慧。
作者简介：张梦霏，女，2000 年生。博士研究生，沉积盆地构造-热演化恢复研究方向。E-mail：mengfeiz0414@163.com。
*通讯作者：邱楠生，男，1968 年生。教授，沉积盆地温压场重建与地热资源评价研究方向。E-mail：qiunsh@cup.edu.cn。常健，男，1982 年生。教授，沉积盆地热演化及油气成藏机理研究方向。E-mail：changjian@cup.edu.cn。

引用本文：张梦霏，邱楠生，常健，冯乾乾，李晨星，刘鑫，龙康杰. 2026. 华南米仓山南缘中生代以来多阶段隆升-剥蚀过程与构造沉积耦合特征. 地质学报，doi：10.19762/j.cnki.dizhixuebao.2025370.
Zhang Mengfei，Qiu Nansheng，Chang Jian，Feng Qianqian，Li Chenxing，Liu Xin，Long Kangjie. 2026. Multistage Mesozoic exhumation-erosion processes and tectono-sedimentary coupling in the southern margin of the Micang Mountain，South China. Acta Geologica Sinica.

映物源区结晶年龄或者沉积地层的最大沉积年龄下限,成为追溯物源演化与构造历史的有力工具(Sircombe, 1999; Li Yingjie et al., 2016; Xu Xianbing et al.,2016; Qian Tao et al.,2023)。通过对比潜在物源区和地层中碎屑锆石 U-Pb 年龄谱图的相似性,能够识别不同物源区的贡献,进而刻画盆缘米仓山隆起的时空变化和构造隆升-剥蚀过程(Zhu Min et al., 2017; 李双建等, 2018; Liu Songnan et al.,2021; Ma Qianli et al.,2021; Qian Tao et al.,2023)。在盆山系统研究中,物源分析侧重于从沉积记录反向推断构造活动时限,可与低温热年代学直接约束的冷却-剥露过程相互补充。源区低温热年代学所反映的冷却-剥露时间,与沉积区碎屑锆石年龄变化的同步性,是识别盆山系统初始耦合过程的关键指标析(Carter and Moss, 1999; Li Yingqiang et al.,2016)。

米仓山隆起位于四川盆地北缘,为华南板块与华北板块相互作用及新生代印度-亚洲板块碰撞过程共同塑造的重要构造单元,记录了多期海侵-海退与构造变形,成为揭示四川盆地构造历史的重要窗口(张茜, 2010; 孙东, 2012)。已有研究揭示了其中生代以来存在多期隆升,但其隆升时间和阶段仍存在争议(田云涛等, 2010; 邓宾等, 2014; Luo Liang, et al.,2014; Zhang Yong et al.,2015; Shao Tongbin et al.,2016; Xu Xianbing et al.,2016; 李双建等, 2018; Berkana et al.,2022; Qian Tao et al.,2023; Tong Kui et al.,2025)。低温热年代学数据显示,米仓山隆起主要经历了两期快速隆升阶段,一期为早侏罗世-早白垩世,另一期始于始新世(Tian Tao et al., 2021; Zhang Yueqiao et al., 2022; 张建勇等, 2024; Tong Kui et al., 2025)。亦有研究提出其中生代快速隆升发生在中侏罗世(田云涛等, 2010; Tian Yuntao et al.,2012; Yang Zhao et al.,2013)或者早白垩世(常远等, 2010; Xu ChangHai et al.,2010);而新生代的快速隆升时间为晚中新世。也有研究补充指出新生代存在始新世中期(约 40 Ma)、渐新世-中新世(23～15 Ma)两期隆升(Tong Kui et al.,2025)。与此同时,物源分析显示在晚三叠世,华北板块与扬子地块沿勉略缝合带发生碰撞,扬子地块内部发生陆内挤压作用,四川盆地北缘三叠纪造山作用强度较低,但发生显著的负荷作用与挠曲沉降。这一构造背景延续至侏罗纪-白垩纪,使区域在构造抬升与持续沉降之间呈现复杂的盆山耦合过程(Luo Liang et al., 2014; Zhang Yong et al., 2015; Shao Tongbin et al., 2016; 李双建等, 2018)。

本文利用米仓山隆起南缘震旦系夹层砂岩和基底花岗岩进行锆石裂变径迹和(U-Th)/He 实验,进行热历史模拟;同时收集了四川盆地北部上三叠统-下侏罗统中碎屑锆石 U-Pb 年龄数据,通过对比样品中主要年龄组分与潜在物源区年龄,识别源区冷却-剥蚀与沉积区物源变化的耦合关系。基于此,建立了米仓山地区自中生代以来多期次隆升-剥蚀过程,限定其初次隆升及盆山系统初始耦合的时限,并探讨了多期构造活动与宏观板块碰撞的关联。研究结果不仅为川北陆内造山的热-动力学机制提供了关键证据,也深化了对秦岭-扬子地块板块拼合演化及盆山耦合作用的认识。

1 地质概况

米仓山隆起位于四川盆地北缘,地处上扬子地块北缘与南秦岭交汇处,整体呈北东向展布。其北侧为秦岭造山带,西侧与龙门山褶皱冲断带相交,东侧与大巴山褶皱冲断带相接,南侧经缓变形区到四川盆地(Dong Yunpeng et al.,2012; Fang Xinyan et al.,2022; 张建勇等, 2024; Tong Kui et al., 2025)。作为典型的中-新生代陆内挤压构造带,米仓山隆起是由太古宙-元古宙基底、新元古代闪长岩、花岗岩、及环绕四周的古生代、中生代沉积岩组成的复式背斜,局部还有新生代沉积物(Yang Zhao et al., 2013; 张文军等, 2016; Berkana et al., 2022; Hui Bo et al.,2025)。其空间结构自北向南可划分为基底隆起区和隆起边缘变形带同时还发育一系列北东走向的逆冲断裂和走滑断裂,从东到西分别为北川-映秀断裂(BYF)、朝天-宁强断裂(CNT)、关帝庙断裂(GDF)、桃园-牟家坝断裂(TMF)、关坝-水磨断裂(GSF)等,构成典型的“基底隆起-盖层滑脱”结构体系(图 1;张国伟等, 1995; Xu Huaming et al., 2009; 张茜, 2010; Tian Yuntao et al.,2012; 彭立勇, 2013; Tong Kui et al., 2025)。

米仓山隆起构造演化受古特提斯、新特提斯及太平洋三大构造域的叠加影响,涉及古特提斯洋形成与关闭、商丹-勉略缝合带发育、新特提斯洋闭合及青藏高原隆升等关键地质事件(Dong Yunpeng et al.,2012; 孙东, 2012; 邓宾等, 2014; Tong Kui et al.,2025)。整体可划分为 4 阶段:前寒武纪基底变形阶段、震旦纪至中三叠世稳定台地阶段、晚三叠世

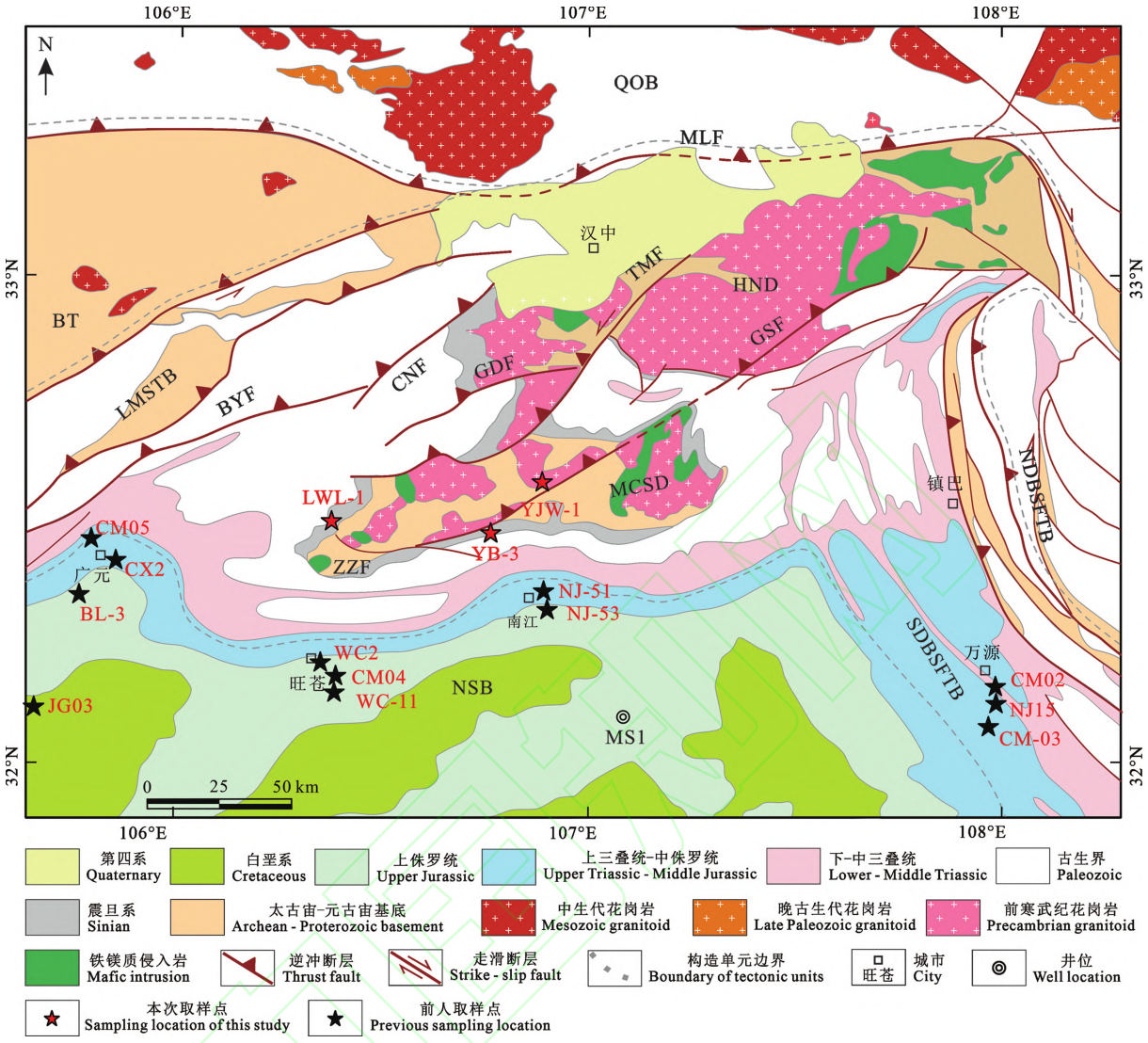

图 1 米仓山区域地质概况图(据 Tong Kui et al.,2025 修改)

Fig. 1 Regional geological overview map of the Micang Mountain (modified after Tong Kui et al.,2025)

QOB—秦岭造山带;BT—碧口地块;NSB—四川盆地北部;HND—汉南穹隆;MCSD—米仓山穹隆;MLF—勉略缝合带;LMSTB—龙门山推覆带;NDBSFTB—北大巴山褶皱冲断带;SDBSFTB—南大巴山褶皱冲断带;BYF—北川-映秀断裂;CNF—朝天-宁强断裂;GDF—关帝庙断裂;GSF—关坝-水磨断裂;QPF—青川-平武断裂;TMF—桃园-牟家坝断裂

QOB—Qinling orogenic belt; BT—Bikou terrane; NSB—northern Sichuan basin; HND—Hannan dome; MCSD—Micangshan dome; MLF—Mianlue suture; LMSTB—Longmenshan thrust belt; NDBSFTB—northern Daba fold-thrust belt; SDBSFTB—Southern Daba fold and thrust belt; BYF—Beichuan-Yingxiu fault; CNF—Chaotian-Ningqiang fault; GDF—Guandimiao fault; GSF—Guanba-Shuimo fault; QPF—Qingchuan-Pingwu fault; TMF—Taoyuan-Mujiaba fault

至白垩纪伴随左行走滑的褶皱冲断阶段,以及晚新生代右行走滑变形阶段(Dong Yunpeng et al.,2012; Tian Tao et al.,2021; Berkana et al.,2022; Tong Kui et al.,2025)。

2 样品与测试方法

2.1 样品采集

本次研究在米仓山南缘地区采集了 3 件样品进行锆石裂变径迹(ZFT)和锆石(U-Th)/He(ZHe)测试,其中 YB-3 和 LWL-3 为震旦系灯三段长石石英砂岩,地层年龄为 551.1～541 Ma(Condon et al.,2005);YJW-1 为基底黑云母花岗岩,锆石 U-Pb 年龄为 838 ± 17 Ma(Zhao Junhong and Zhou Meifu, 2009),具体采集位置见图 1,样品采集信息见表 1,同时还收集了前人已经发表的部分样品数据信息以构建完整数据集。

2.2 锆石裂变径迹测年

锆石裂变径迹年龄是在中国石油大学(北京)热年代学实验室测试。实验采用裂变径迹全自动系统(包括 Zeiss Axio-Imager M2m 全显微镜和 TackWork3.0

表 1 米仓山隆起南缘样品基本地质信息

Table 1 Basicgeological information of samples from the southern margin of the Micang Mountain uplift

序号	样品号	经纬度	海拔(m)	岩性	测试方法	文献
1	YB-3	106.782°E, 32.469°N	755	震旦系砂岩	ZFT、ZHe	本文
2	LWL-1	106.391°E, 32.507°N	1289	震旦系砂岩	ZFT、ZHe	本文
3	YJW-1	106.928°E, 32.557°N	1411	元古宙花岗岩	ZFT、ZHe	本文
4	MC-7	106.878°E, 32.527°N	659	元古宙闪长岩	AFT、ZFT	Tong Kui et al.,2025
5	MC-8	106.845°E, 32.590°N	1269	元古宙闪长岩	AFT、ZFT	Tong Kui et al.,2025
6	MC-9	106.834°E, 32.620°N	1654	元古宙花岗岩	AFT、ZFT	Tong Kui et al.,2025
7	MC-11	107.591°E, 32.961°N	498	元古宙闪长岩	AFT、ZFT	Tong Kui et al.,2025
8	MC-14	107.41°E, 33.099°N	580	元古宙花岗岩	AFT、ZFT	Tong Kui et al.,2025
9	MC-15	106.456°E, 32.482°N	619	元古宙闪长岩	AFT、ZFT	Tong Kui et al.,2025
10	MC-17	106.446°E, 32.472°N	625	元古宙花岗岩	AFT、ZFT	Tong Kui et al.,2025
11	WG-01	106.477°E, 32.532°N	763	新元古代闪长岩	AFT、ZHe	张建勇等, 2024
12	WG-05	106.476°E, 32.541°N	1049	震旦系含砾砂岩	AFT、ZHe	张建勇等, 2024
13	WG-10	106.484°E, 32.586°N	912	震旦系含砾砂岩	AFT、ZHe	张建勇等, 2024
14	GWS-01	106.801°E, 32.669°N	994	元古宙花岗岩	ZHe	张建勇等, 2024

操作软件)、NWR 193nm Excimer 激光剥蚀系统(LA)和 Agilent 7900 电感耦合等离子体质谱仪(ICP-MS)进行。测试实验主要步骤为:① 将样品粉碎、筛选、磁选和重液分选获得锆石颗粒;② 利用 Teflon 薄片安装、固定锆石,制成 ZFT 样品靶;③ 对锆石颗粒进行研磨和抛光;④ 按 KOH 11.2 g 与 NaOH8 g 的重量比混合二者,在 228℃温度下蚀刻锆石样品,蚀刻时间为 8～10 h;⑤ 观察蚀刻好的颗粒,统计其自发径迹数;⑥ 选用 FCT 标准锆石作为标准样品,利用 LA-ICP-MS 系统测量颗粒表面径迹统计区域^{238}U 含量;⑦ 根据裂变径迹公式计算裂变径迹年龄。

相较于传统外探测器法,原位 LA-ICP-MS 裂变径迹定年通过激光剥蚀直接测定矿物 ^{238}U 含量,省去了中子辐照与云母外探测器记录诱发径迹的复杂流程,从而大幅提高实验安全性与效率;传统方法不仅存在辐照安全风险,还需等待样品辐射衰减,周期显著更长。同时,LA-ICP-MS 法能有效避免因人为挑选自发径迹和诱发径迹比值相近的颗粒而造成人为地降低年龄分散性的问题(李晨星等, 2025)。然而,当矿物晶体内部铀含量分布不均匀时,LA-ICP-MS 法可能造成铀含量测试结果与实际产生径迹的有效铀含量差异较大,造成裂变径迹年龄误差增加(Donelick et al.,2005; Cogné et al.,2020)。

2.3 锆石(U-Th)/He 测年

锆石(U-Th)/He 年龄也是在中国石油大学(北京)热年代学实验室测试。测试实验主要包括以下几个步骤:① 将分选好的锆石颗粒放入在薄片上在光学显微镜下,对每个样品挑选出 5 颗自形锆石颗粒,尽量确保颗粒不含包裹体,并利用 VideoTest3 软件,观察并测量颗粒的长度、宽度和锥高,相应做好编号;② 使用 1 mm×1 mm 的金属铌囊包裹锆石颗粒,用 Alphachron MK II 氦提取测量仪进行矿物 He 含量测试,用国际上通用的鱼谷凝灰岩锆石(Fish Canyon Tuff Zircon,简称 FCT 锆石)作为实验标准样品;③ 锆石颗粒 He 含量测试完后,将包裹颗粒的铌囊从氦提取测量仪中取出,放入 PFA(铁氟龙)瓶中,依次加入 25 μL 浓度已知的^{230}Th、^{235}U 同位素稀释剂、50 μL 硝酸溶液(HNO_3)溶液和 300 μL 氢氟酸溶液(HF),标准压力下采用消解技术溶解样品,使用 Agilent7900 电感耦合等离子质谱仪进行 U、Th 浓度测试;④ 用 IsoplotR 计算锆石颗粒(U-Th)/He 年龄,同时根据 Gautheron and Tassan-Got(2010)提出计算模型对年龄结果进行校正。

3 热史测试结果

3.1 锆石裂变径迹年龄

锆石裂变径迹年龄测试结果见表 2。YB-3 样品的 ZFT 中值年龄为 370±32 Ma(图 2a),LWL-1 样品的 ZFT 中值年龄为 399±39 Ma(图 2b),两者均远小于地层年龄;YJW-1 样品的 ZFT 中值年龄为 277±27 Ma(图 2c),远小于其结晶年龄。三个样品的 P(χ^2)检验值都大于 5%,表明单颗粒年龄属于同一组年龄,较为集中;同时 ZFT 年龄均小于地层年龄或结晶年龄,表明这些样品均经历过全部退火,其年龄可以有效揭示米仓山隆起中生代以来的构造演化(Green, 1981; Galbraith and Laslett, 1993)。还收集了部分前人已经发表的数据,相关部分数据汇总见表 2,表 3。

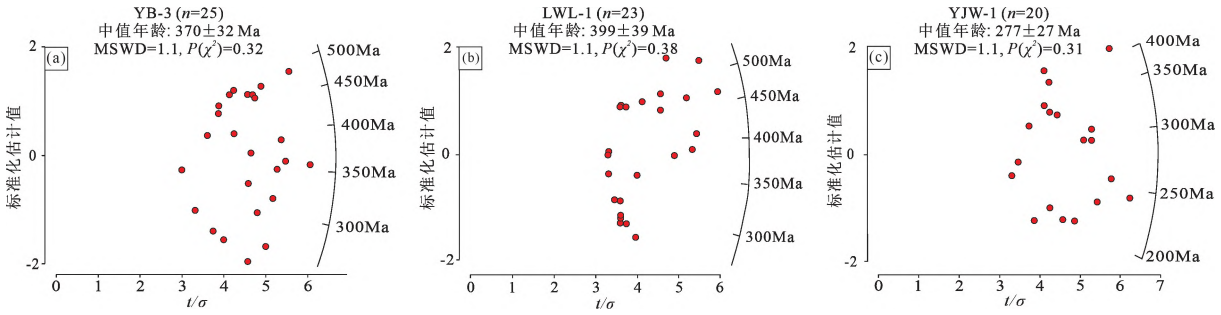

图 2 米仓山隆起南缘样品单颗粒裂变径迹年龄雷达图

Fig. 2 The radar chart of zircon fission track grain ages from samples at the southern margin of the Micang Mountain uplift

表 2 米仓山隆起南缘样品锆石裂变径迹年龄测试结果

Table 2 Zircon fission track age determination results of samples from the southern margin of the Micang Mountain uplift

样品号	颗粒数(n)	ρ_s($\times10^5$/cm^2)(N_s)	ρ_i($\times10^5$/cm^2)(N_i)	ρ_d($\times10^5$/cm^2)(N_d)	U($\times10^{-6}$)	$P(\chi^2)$(%)	中值年龄(Ma)	±1σ(Ma)
YB-3	28	212.5(810)	/	/	126.69	32	370	32
LWL-1	24	263.3(449)	/	/	137.59	38	399	39
YJW-1	24	238.3(526)	/	/	180.14	31	277	27
MC-7	24	198.7(9765)	31.2 (1535)	6.7(4630)	170.39	0	177	8
MC-8	24	196.9(5728)	35.2(1024)	6.7(4630)	187.58	0.30	159	8
MC-9	24	218.8(6108)	43.3(1210)	6.6 (4630)	242.66	23.00	141	8
MC-11	24	215.8(12516)	38.1(2209)	6.5(4630)	214.19	0	154	5
MC-14	20	151.1(4144)	19.7(540)	6.4 (4630)	112.06	0.60	208	14
MC-15	9	178.2 (2295)	28.4(366)	6.3(4630)	157.70	35.70	168	13
MC-17	24	211.3(8453)	27.3(1094)	6.2 (4630)	160.26	3.30	202	8

注:ρ_s 表示锆石自发径迹密度;N_s 表示锆石自发径迹数;ρ_i 表示诱发径迹密度;N_i 表示诱发径迹数目;ρ_d 表示标准铀玻璃种的径迹密度;N_d 表示标准玻璃上的诱发径迹数目;$P(\chi^2)$表示卡方检验,$P(\chi^2)>0.05$,年龄为中值年龄。

表 3 米仓山隆起南缘样品磷灰石裂变径迹年龄测试结果

Table 3 Apatite fission track age determination results of samples from the southern margin of the Micang Mountain uplift

样品号	颗粒数(n)	ρ_s($\times10^5$/cm^2)(N_s)	ρ_i($\times10^5$/cm^2)(N_i)	ρ_d($\times10^5$/cm^2)(N_d)	$P(\chi^2)$(%)	中值年龄(Ma)	平均径迹长度(±1σ,μm)(N)	D_{par}(±1σ,μm)
WG-01	15	9.63(312)	19.136(620)	15.4(20 410)	95.2	106.1±7.8	11.58±1.35(34)	2.75±0.37
WG-05	19	9.88(493)	18.978(947)	15.7(19 409)	99	111.8±6.7	11.82±1.46(64)	2.40±0.43
WG-10	20	8.978(457)	15.265(777)	15.0(19 575)	99.5	120.6±7.7	12.75±1.22(58)	2.20±0.26
MC-7	28	6.124(1222)	20.366(4064)	10.067(5867)	0	58±5	12.1±1.8(57)	/
MC-8	28	9.288(2602)	18.211(5102)	9.97(5867)	16.4	98±6	12.5±1.8(93)	/
MC-9	28	5.149(1193)	9.957(2307)	9.874(5867)	41.6	99±6	12.5±1.8(122)	/
MC-11	22	11.399(1729)	26.563(4029)	9.681(5867)	46	80±5	12.7±2.1(100)	/
MC-14	28	2.964(1352)	4.63(2112)	9.488(5867)	80.8	117±7	13.3±1.8(110)	/
MC-15	28	9.505(683)	21.835(1569)	9.392(5867)	87.3	79±5	12.4±1.9(71)	/
MC-17	27	2.765(602)	6.214(1353)	9.199(5867)	90.1	79±6	12.3±1.9(104)	/

注:ρ_s 表示锆石自发径迹密度;N_s 表示锆石自发径迹数;ρ_i 表示诱发径迹密度;N_i 表示诱发径迹数目;ρ_d 表示标准铀玻璃种的径迹密度;N_d 表示标准玻璃上的诱发径迹数目;$P(\chi^2)$表示卡方检验,$P(\chi^2)>0.05$,年龄为中值年龄。

3.2 锆石(U-Th)/He 年龄

锆石(U-Th)/He 年龄测试结果见表 4。YB-3 样品的锆石(U-Th)/He 年龄变化较大(图 3),介于 158.1±7.9～290.0±14.5 Ma,这可能与辐射损伤或者是否含 He 的包裹体有关(Guenthner et al.,2013)。其可明显分为两组,YB-3-3 和 YB-3-4 年龄相对集中,介于 287.7±14.4～290.0±14.5 Ma,均值年龄为 288.8±14.4 Ma;YB-3-1、YB-3-2 和 YB-3-5 三个样品的年龄相对集中,介于 158.1±7.9～178.9±8.9 Ma,均值年龄为 168.0±8.4 Ma,两组年龄均远小于地层年龄。LWL-1 样品的锆石(U-Th)/He 年龄比较集中,介于 139.9±7.0～196.9±9.9 Ma,均值年龄为 159.0±8.0 Ma,其年龄远小于地层年龄。而 YJW-1 样品的锆石(U-Th)/He 年龄介于 136.4±6.8～142.0±7.1 Ma,均值年龄介于 139.6±7.0 Ma,远小于其岩体年龄 814±9 Ma。

收集的部分前人已经发表的 ZHe 数据见表 4。

YB-3 样品单颗粒锆石(U-Th)/He 年龄和有效 U 含量、颗粒半径呈负相关关系;LWL-1 样品单颗粒锆石(U-Th)/He 年龄和有效 U 含量呈负相关关系,而与颗粒半径呈正相关关系;YJW-1 样品单颗粒锆石(U-Th)/He 年龄和有效 U 含量关系不明显,而与颗粒半径呈负相关关系(图 3)。三个样品的单颗粒年龄表现出较强的分散性,主要是由辐射损伤造成的,且年龄都远小于地层年龄或者结晶年龄,表明其沉积后经过高温 He 扩散,样品所经历的最大古温度超过了 ZHe 的封闭温度(200℃)(Guenthner et al.,2013)。

表 4 米仓山隆起南缘样品锆石(U-Th)/He 年龄测试结果

Table 4 Zircon (U-Th)/He age determination results of samples from the southern margin of the Micang Mountainuplift

样品号	颗粒号	半径 (μm)	^{4}He (nmol/g)	颗粒质量 (μg)	U ($\times10^{-6}$)	Th ($\times10^{-6}$)	eU	年龄 (Ma)	FT	校正年龄 (Ma)	±1σ(Ma)
YB-3	YB-3-1	98.1	49.9	31.9	51.1	37.5	178.9	152.4	0.85	178.9	8.9
	YB-3-2	76.3	29.7	19.0	34.9	28.6	158.1	130.9	0.83	158.1	7.9
	YB-3-3	73.9	68.9	16.1	42.02	44.1	290.0	239.2	0.83	290.0	14.5
	YB-3-4	53.2	84.5	5.3	59.04	58.2	287.7	211.4	0.74	287.7	14.4
	YB-3-5	61.8	68.4	8.3	79.5	76.5	167.1	128.7	0.77	167.1	8.4
YJW-1	YJW-1-1	52.5	42.7	6.1	68.4	44.6	78.6	99.8	0.73	136.4	6.8
	YJW-1-2	40.6	70.7	3.2	121.5	80.8	140.1	92.5	0.66	140.1	7.0
	YJW-1-3	40.2	34.0	3.8	55.8	40.3	65.1	96.0	0.68	142.0	7.1
	YJW-1-4	47.5	82.7	4.5	133.1	90.7	154.0	98.7	0.71	139.7	7.0
LWL-1	LWL-1-1	45.4	26.6	3.3	41.1	28.7	47.6	102.1	0.69	147.4	7.4
	LWL-1-2	40.4	61.2	2.5	107.3	63.2	121.8	92.0	0.66	139.9	7.0
	LWL-1-3	32.4	31.5	1.6	52.7	54.2	65.1	88.6	0.58	152.0	7.6
	LWL-1-4	44.3	20.7	3.5	19.7	30.4	26.7	141.0	0.72	196.9	9.9
WG-10	WG-10-1	71.9	56.6	12.2	147.0	221.8	199.1	/	0.81	175.5	10.9
	WG-10-2	63.4	31.1	7.0	162.4	110.2	188.3	/	0.79	189.3	11.7
GWS-01	GWS-01-1	64.8	26.0	9.4	139.4	84.0	159.1	/	0.80	140.6	8.7
	GWS-01-2	62.0	22.5	6.0	186.9	136.9	219.1	/	0.79	138.1	8.6
	GWS-01-3	55.0	37.8	5.4	320.7	188.0	364.9	/	0.76	155.1	9.6
WG-05	WG-05-1	54.5	18.6	4.4	151.6	124.6	180.9	/	0.76	189.9	11.8
	WG-05-2	56.6	12.8	3.8	127.5	109.2	153.1	/	0.76	178.2	11.0
	WG-05-3	54.0	21.3	5.3	154.4	80.2	173.3	/	0.76	186.9	11.6

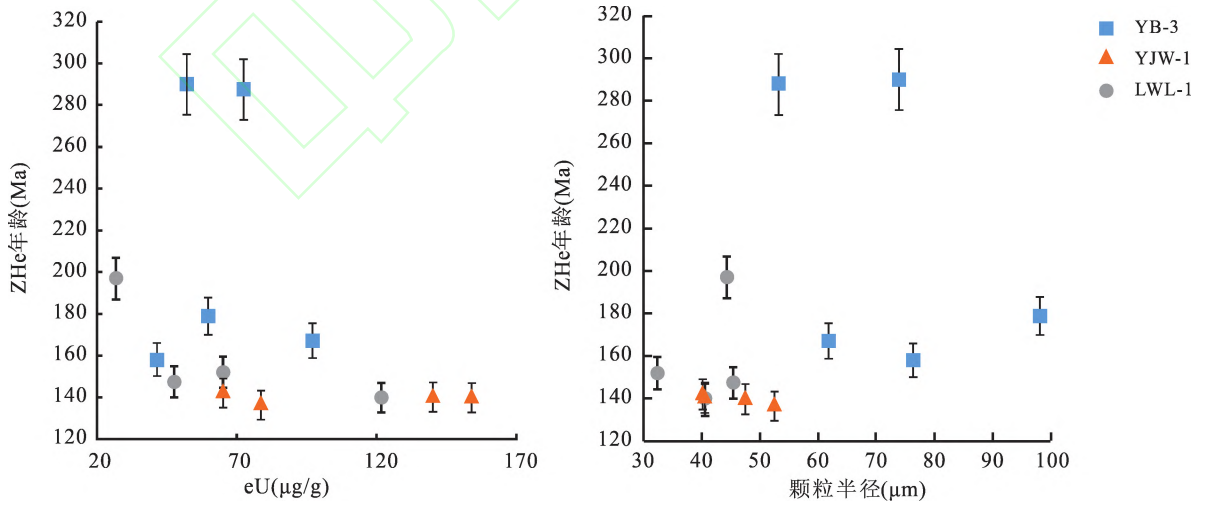

图 3 米仓山南缘锆石(U-Th)/He 年龄和有效铀含量、颗粒半径关系图

Fig. 3 Relationship diagram of zircon (U-Th)/He ages with eU and grain radius from the southern margin of the Micang Mountain

3.3 热史模拟结果

在对研究区的各种古温标进行定性分析的基础上,依据 ZFT、ZHe 年龄等古温标对样品的热演化史进行了模拟,其中 ZFT 模拟采用平行曲线模型

(Yamada et al.,2007),ZHe 模拟采用 ZRDAAM 模型(Gautheron et al.,2013)。利用 HeFty 软件(2.1.7 版本)并基于蒙特卡洛法随机模拟了 10000 条热演化史,其中,"最好"的温度路径代表了该样品的热演化史。拟合优度(GOF)值代表模拟计算的年龄与实测年龄的拟合程度,当 GOF 大于 50%,说明热演化史模拟结果是可靠的。

对于 YB-3 和 LWL-3 砂岩样品,其热史模拟开始的时间设置为样品开始沉积的时间,沉积时的地表温度和现今地层温度均设为 20±5℃。为了获得更可靠的热史路径,根据研究区沉积层系间发育的不整合面、构造演化成果、结合的低温热年代学参数,设置了多个约束条件(图 4)。其中根据 ZHe 年龄设置了中-晚侏罗世的约束条件,结合不整合面发育程度和研究区构造演化设置了早泥盆世、中-晚三叠世和早二叠世三个约束条件,而中新世约束条件是根据前人热史成果设置的(张建勇等, 2024; Tong Kui et al.,2025)。三个样品都得热史模拟都得到了较好的结果,最佳拟合度都大于 50%。

样品 YB-3 和 LWL-1 热史模拟结果揭示了米仓山地区自中生代以来经历了四个阶段抬升冷却过程(图 4a、b):① 晚三叠世至中侏罗世(230～160 Ma)的缓慢冷却抬升阶段,地层温度从 240℃逐步降至 200℃,冷却速率约为 0.57 ℃/Ma;② 晚侏罗世-早白垩世(160～120 Ma),快速冷却隆升阶段,地层温度从 200℃骤降至 70℃,冷却速率约为 3.25 ℃/Ma;③ 晚白垩世-中新世(120～20 Ma)处于构造平稳阶段,温度降低幅度较小,冷却速率为 0.2 ℃/Ma;④ 中新世(20 Ma)以来的末次快速隆升,地层温度下降至地表温度冷却速率约为 1.5 ℃/Ma。YJW-1 样品热史分析也表明(图 4c),米仓山地区晚三叠世以来的构造抬升阶段与 YB-3、LWL-1 样品热史结果一致。

4 米仓山南缘中生代地层物源分析

4.1 潜在物源

通过四川盆地北部中-新生代陆相地层特征及其周缘造山带构造演化过程,可识别出其潜在的物源为华北克拉通南缘、北秦岭造山带、南秦岭造山带、扬子地块北缘、龙门山褶皱带和松潘-甘孜地区等(Shi Yu et al.,2013; Shao Tongbin et al.,2016; 张勇, 2016; 李双建等, 2018; Liu Songnan et al., 2021; Qian Tao et al.,2023)。

华北克拉通南缘由太古宙至元古宙变质基底与中元古代至新生代未变质地层组成,广泛出露新太古代至中元古代岩体,其碎屑锆石年龄谱显示两个主要峰值:最老峰值为～2510 Ma,次老峰值为～1867 Ma,缺乏 900～700 Ma 年龄分布(图 5a);受华北与华南板块碰撞影响,最年轻锆石年龄可更新至 270 Ma(Li Hongyan et al.,2010; Shi Yu et al, 2013; Zhu Xiaoqing et al.,2014; 张勇, 2016)。秦岭造山带呈东西向夹于华北与华南板块之间,被商丹缝合带分为北秦岭与南秦岭两带,北秦岭碎屑锆石年龄谱以～927 Ma 为主峰,伴～410 Ma 次峰(图 5b; Shi Yu et al, 2013; 张勇, 2016);南秦岭(包括北大巴山地区)则以～750 Ma 和～460 Ma 为两大年龄峰值(图 5c, Shi Yu et al, 2013)。上扬子北缘紧邻南秦岭,包括汉南-米仓山隆起,其碎屑锆石年龄谱呈现三个主峰:～2683 Ma、～2000 Ma 和～788 Ma(图 5d),其中新元古代岩浆活动是上扬子地块北缘地壳增厚显著代表事件(Shi Yu et al.,2013; 张勇, 2016)。龙门山褶皱带位于四川盆地西侧,主要由未变形的古生代被动陆缘碳酸盐沉积及前寒武结晶基底构成,碎屑锆石年龄谱具～2500 Ma、～950 Ma 和～500 Ma 三个峰值(图 5e; Duan Liang et al.,2011; Chen Qiong et al.,2016; 张勇, 2016)。松潘-甘孜地区位于龙门山褶皱带以西,为古特提斯洋俯冲形成的增生楔加积体,地表以三叠世复理石沉积为主,其碎屑锆石年龄谱包含两个主峰和四个次峰,分别为～2500 Ma,～1864 Ma,～761 Ma,～437 Ma,～272 Ma 和～229 Ma(图 5f; Bruguier et al., 1997; Weislogel et al.,2006; 张勇, 2016; 刘祥等, 2021)。

4.2 上三叠统须家河组碎屑锆石 U-Pb 年龄特征

四川盆地北部地区上三叠统须家河组碎屑锆石年龄谱图呈现出明显的多峰特征,主要包括五个显著年龄峰值:～2460 Ma,～1868 Ma,～806 Ma,～457 Ma 和～230 Ma,各峰值年龄对应的物源存在显著差异(图 6)。古元古代早期到古元古代晚期(～2470 Ma 和～1870 Ma)的锆石占比最高,约为 50%;新元古代(～806 Ma)锆石占比约为 26%;古生代(～457 Ma)锆石占比最低,约为 7%;最年轻的中生代峰值(～230 Ma)锆石占比约为 12%(Luo Liang et al.,2014; Zhang Yong et al.,2015; Shao Tongbin et al.,2016; 李双建等, 2018)。

4.3 下侏罗统白田坝组碎屑锆石 U-Pb 年龄特征

四川盆地北部地区下侏罗统白田坝组碎屑锆石

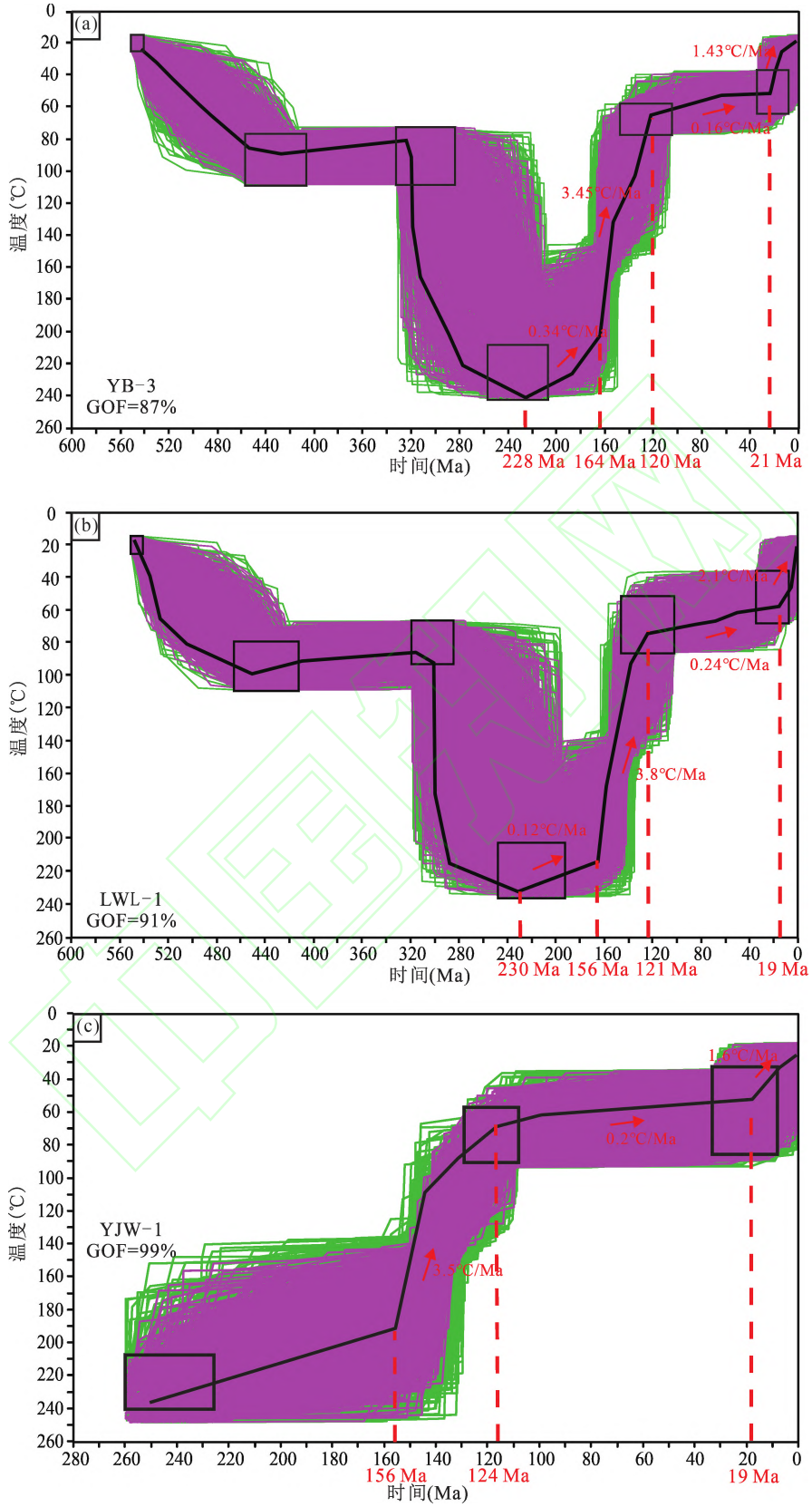

图 4 米仓山隆起南缘震旦系样品热史模拟结果

Fig. 4 Thermal history simulation results of Precambrian samples from the southern margin of the Micang Mountain uplift

绿线、紫线、黑线分别代表可接受、好的、最佳热史路径

The green, purple, and black lines represent the acceptable, good, and optimal thermal history paths, respectively

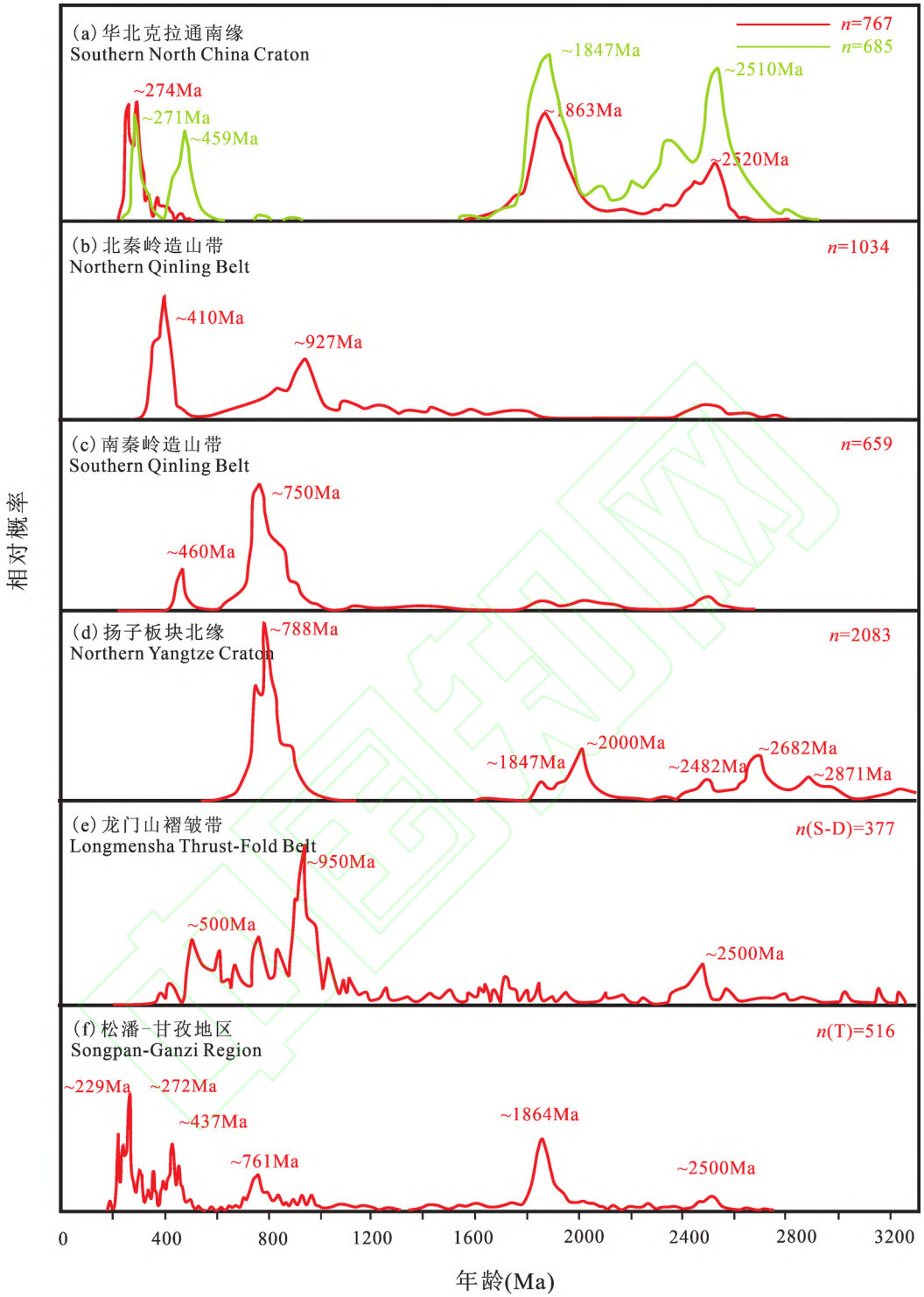

图 5 米仓山隆起南缘周围潜在物源区锆石年龄谱图(据张勇, 2016, 刘祥等, 2021)

Fig. 5 Zircon age spectrum of potential provenance areas surrounding the Micang Mountain uplift (after Zhang Yong, 2016; Liu Xiang et al. ,2021)

年龄分布与上三叠统须家河组碎屑锆石年龄谱图具有相似性,也出现多组峰值,分别为～2481 Ma,～1849 Ma,～801 Ma,～448 Ma,～214 Ma(图 7)。古元古代早期到古元古代晚期(～2481 Ma 和～1849 Ma)的锆石占比约为 18.3%;新元古代晚期(～801 Ma)锆石占比最高,约为 55.7%;早古生代(～448 Ma)锆石占比约为 13.7%。最年轻的峰值(～214 Ma)锆石占比最低,约为 12.3%(Shao Tongbin et al. ,2016; 李双建等, 2018; Qian Tao et al. ,2023)。

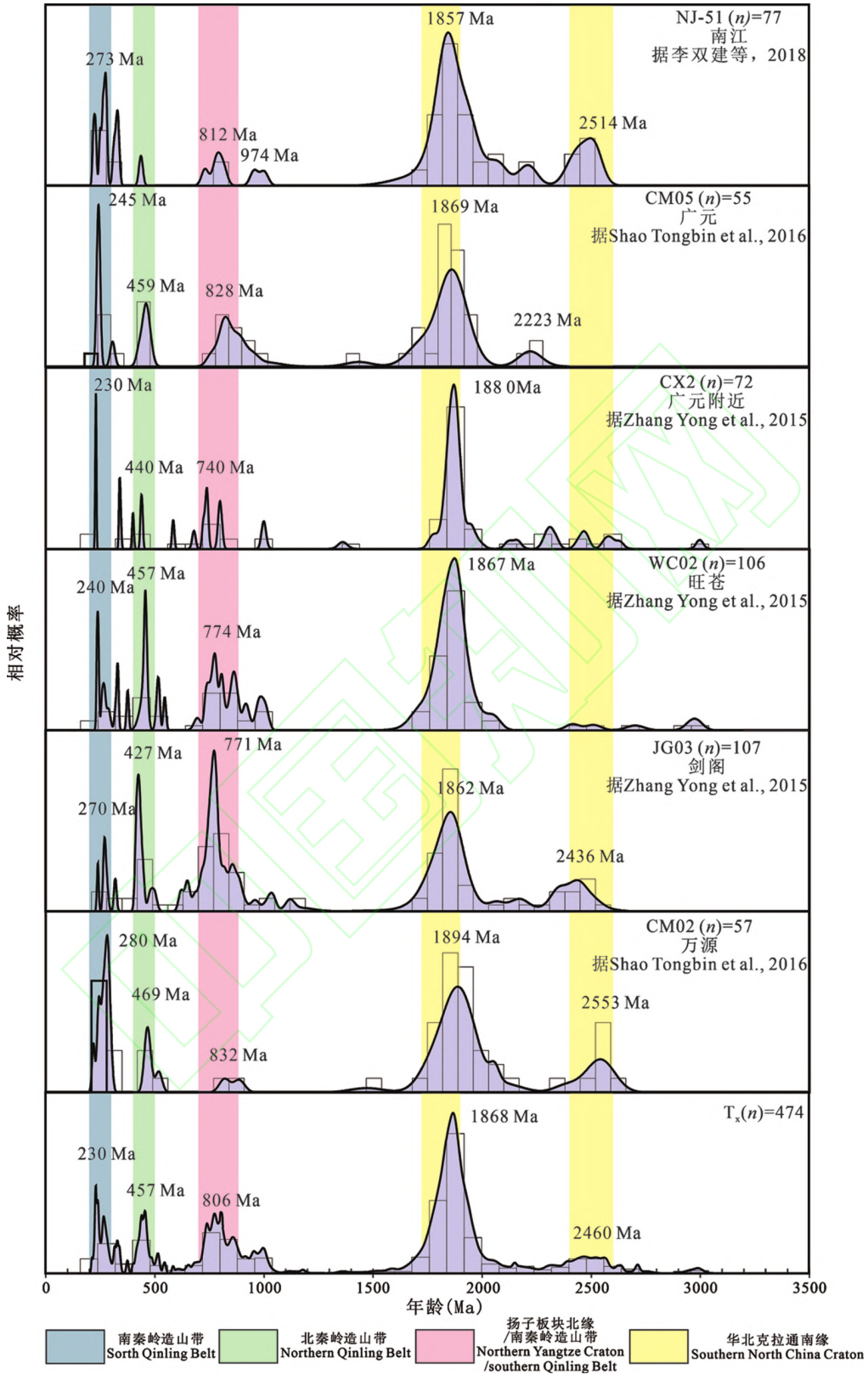

图 6 四川盆地北部晚三叠世须家河组锆石 U-Pb 年龄分布直方图(数据来源 Luo Liang et al.,2014; Zhang Yong et al.,2015; Shao Tongbin et al.,2016; 李双建等, 2018)

Fig. 6 Histogram of zircon U-Pb age distribution in the late Triassic Xujiahe Formation at the southern margin of the Micang Mountain uplift (data sources: Luo Liang et al.,2014; Zhang Yong et al.,2015; Shao Tongbin et al.,2016; Li Shuangjian et al.,2018)

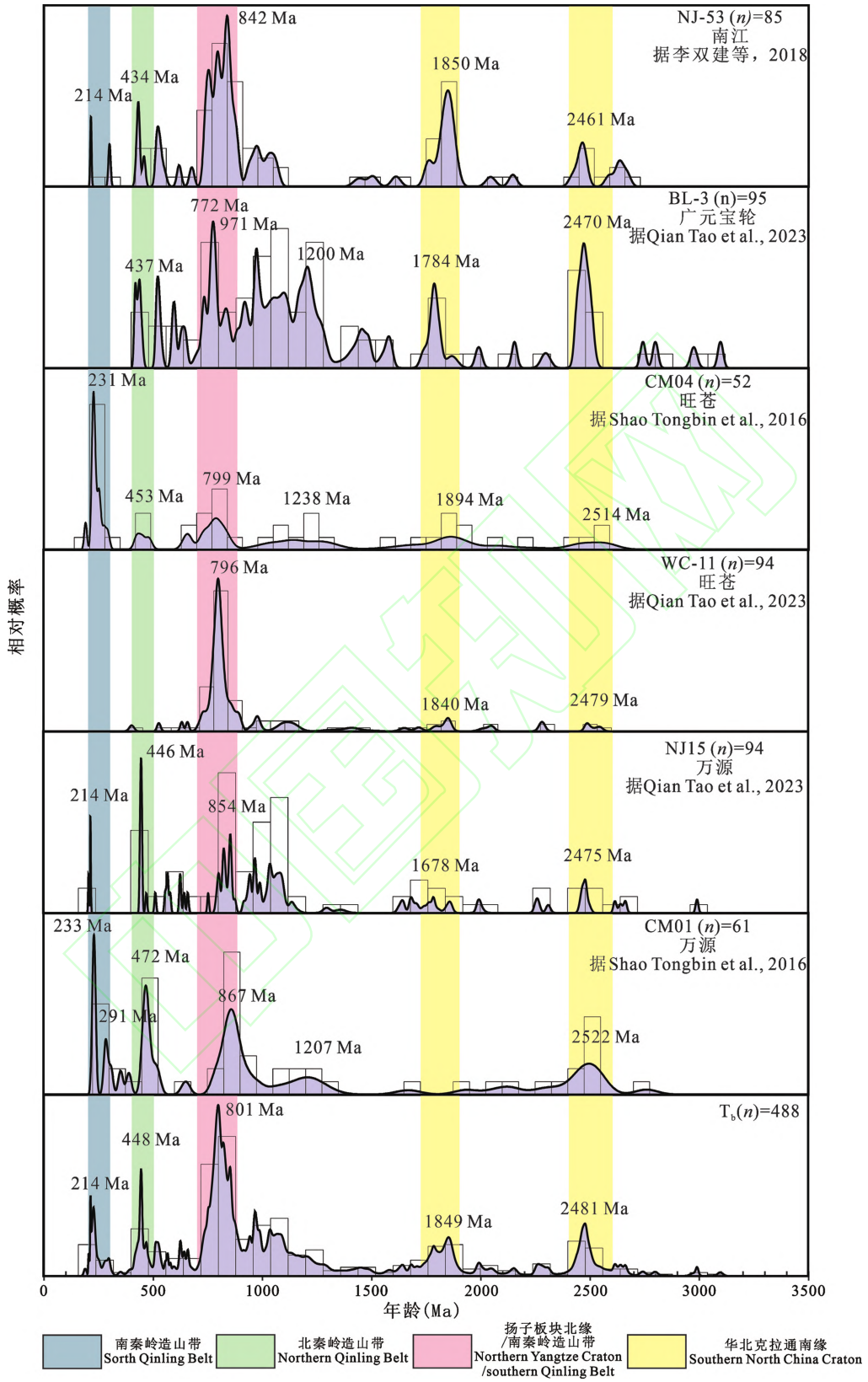

图 7　四川盆地北部侏罗世地层锆石 U-Pb 年龄分布直方图(数据来源 Shao Tongbin et al.,2016；李双建等，2018；Qian Tao et al.,2023)

Fig. 7　Histogram of zircon U-Pb age distribution in Jurassic strata at the southern margin of the Micang Mountain uplift (data sources: Shao et al.,2016; Li Shuangjian et al.,2018; Qian Tao et al.,2023)

5 讨论

5.1 多阶段隆升的动力学机制与区域构造演化

米仓山隆起自前寒武纪以来的多阶段构造演化,清晰地记录了扬子地块北缘对特提斯构造域闭合、古太平洋板块俯冲与青藏高原东向生长的构造响应(Xu Huaming et al.,2009; 田云涛等, 2010; 何登发等, 2011,2025; Yang Zhao et al.,2013; Berkana et al.,2022; 张建勇等, 2024; Tong Kui et al.,2025)。本文通过低温热年代学约束与构造解释结合的方法,重建了米仓山隆起自中生代以来的完整演化序列,其构造变形特征呈现出显著的阶段性和动力学差异,可分为碰撞前期,同碰撞期、快速碰撞隆升期、短暂构造停滞期、构造叠加和整体隆升期。

5.1.1 碰撞前期(晚三叠世以前)

晚古生代,由于华南板块从冈瓦纳大陆地块北缘裂解、漂移,扬子地块北缘成为面向古特提斯洋的被动大陆板块边缘,持续接受浅海沉积(张国伟等, 1995; 何登发等, 2011; Dong Yunpeng et al., 2021; Huang Hanyu et al.,2024; Tong Kui et al., 2025)。晚二叠世,勉略洋向南秦岭地块俯冲并自东向西逐渐穿时关闭(图 8a;张国伟等, 1995; Meng Qingren et al., 2005; Lai Shaocong and Qin Jiangfeng, 2010; 孙东, 2012; Wu Yuanbao and Zheng Yongfei, 2013; 董云鹏等,2022;许军等, 2024; 王启航, 2025)。导致扬子地块北缘进入快速沉降阶段,温度持续升高。进入中三叠世期间,随着勉略洋完全消亡,扬子地块开始(Dong Yunpeng et al., 2011; Ma Qianli et al., 2021; Zheng Binsong et al.,2021),与早期拼贴于华北板块的秦岭地块发生点碰撞(Zhang Kaijun, 1997; Liu Shaofeng et al., 2001; 张国伟等, 2003; Dong Yunpeng et al.,2011; 孙东, 2012)。此时,扬子地块向秦岭地块俯冲,区域构造格局初步形成(Meng Qingren and Zhang Guowei, 1999; 李岩峰等, 2008; Dong Yunpeng et al.,2011; 朱晨曦, 2023),灯影组地层温度也达到了峰值(220~240℃)。

5.1.2 同碰撞期(晚三叠世-中侏罗世)

晚三叠世至中侏罗世(230~160 Ma)期间,米仓山地区进入缓慢抬升与冷却阶段,与扬子地块向秦岭地块的俯冲密切相关。古太平洋向西迁移并开始向欧亚大陆下俯冲(何登发等, 2011; Valer'evna等, 2017; Dong Yunpeng et al.,2021)。同时,扬子地块和秦岭地块也发生强烈的陆-陆碰撞,秦岭造山带由北向南快速隆升,引发扬子地块发生广泛海退,四川盆地由海相沉积体系转变为陆相沉积体系(张茜, 2010; Dong Yunpeng et al.,2011; 张文军等, 2016; 朱晨曦, 2023)。受上扬子地块底部的刚性基底的阻挡缓冲,此时造山变形只波及到汉南隆起的南缘(张茜, 2010; 孙东, 2012)。米仓山地区由于远离秦岭造山带,并未发生大规模的逆冲隆升,但也受到远程构造效应的影响,发育低幅度的水下隆起,并在残余海湾背景下持续接受沉积(图 8b,张茜, 2010; 何登发等, 2011; 孙东, 2012; Li Jinxi et al.,2015)。随着秦岭造山带的持续挤压,米仓山地区缓慢抬升,幅度小,速率慢,直到中侏罗世,地层温度逐步降至 200℃,冷却速率约为 0.57 ℃/Ma(图 8c)。

5.1.3 快速碰撞隆升期(晚侏罗世-早白垩世)

侏罗世至早白垩世期间(160~120 Ma),米仓山地区进入快速冷却隆升阶段,与扬子地块快速向下俯冲相关。太平洋板块持续西向俯冲于欧亚板块之下,扬子地块也持续向秦岭地块快速俯冲楔入,秦岭造山带发生强烈的陆内俯冲和逆冲推覆构造(何登发等, 2011; 侯方辉, 2015; Li Yingqiang et al., 2016; Valer'evna et al.,2017)。刚性勉略缝合带使扬子地块北缘俯冲角度变陡(Xu ChangHai et al., 2010; 李三忠等, 2011; Valer'evna et al.,2017; Zhang Yueqiao et al.,2022; 王启航, 2025),导致米仓山地区发生强烈陆内缩短,挤压隆升活动持续加强,前陆深层断裂系统进一步发育,形成由北向南的冲断褶皱系统(陈竹新等, 2008, 2019; 常远等, 2010; 张茜, 2010; 朱晨曦, 2023)。随后发育北东向走滑断裂,并左旋错断前期的东西向构造体系(孙东, 2012; Tian Tao et al.,2021)。此阶段,米仓山地区快速隆升降温,地层温度从 200℃骤降至 70℃,隆升速率显著加快,冷却速率高达 3.25 ℃/Ma,远超晚三叠世-中侏罗世时期。此外,板块运动学模型显示,扬子地块在俯冲时,相对华北板块 NWW 向移动,构造叠加加剧陆内挤压变形作用,米仓山隆起主体构造基本定型(图 8d,张国伟等, 2003,2004; 张茜, 2010; 孙东, 2012; Li Jinxi et al.,2015)。

5.1.4 短暂构造停滞期(晚白垩世-中新世)

晚白垩世至中新世(120~20 Ma)期间,米仓山地区进入构造平稳与热史停滞阶段,与陆内造山作用减弱和区域应力改变密切相关。扬子地块和秦岭地块主碰撞阶段结束后,区域进入陆内造山阶段,形

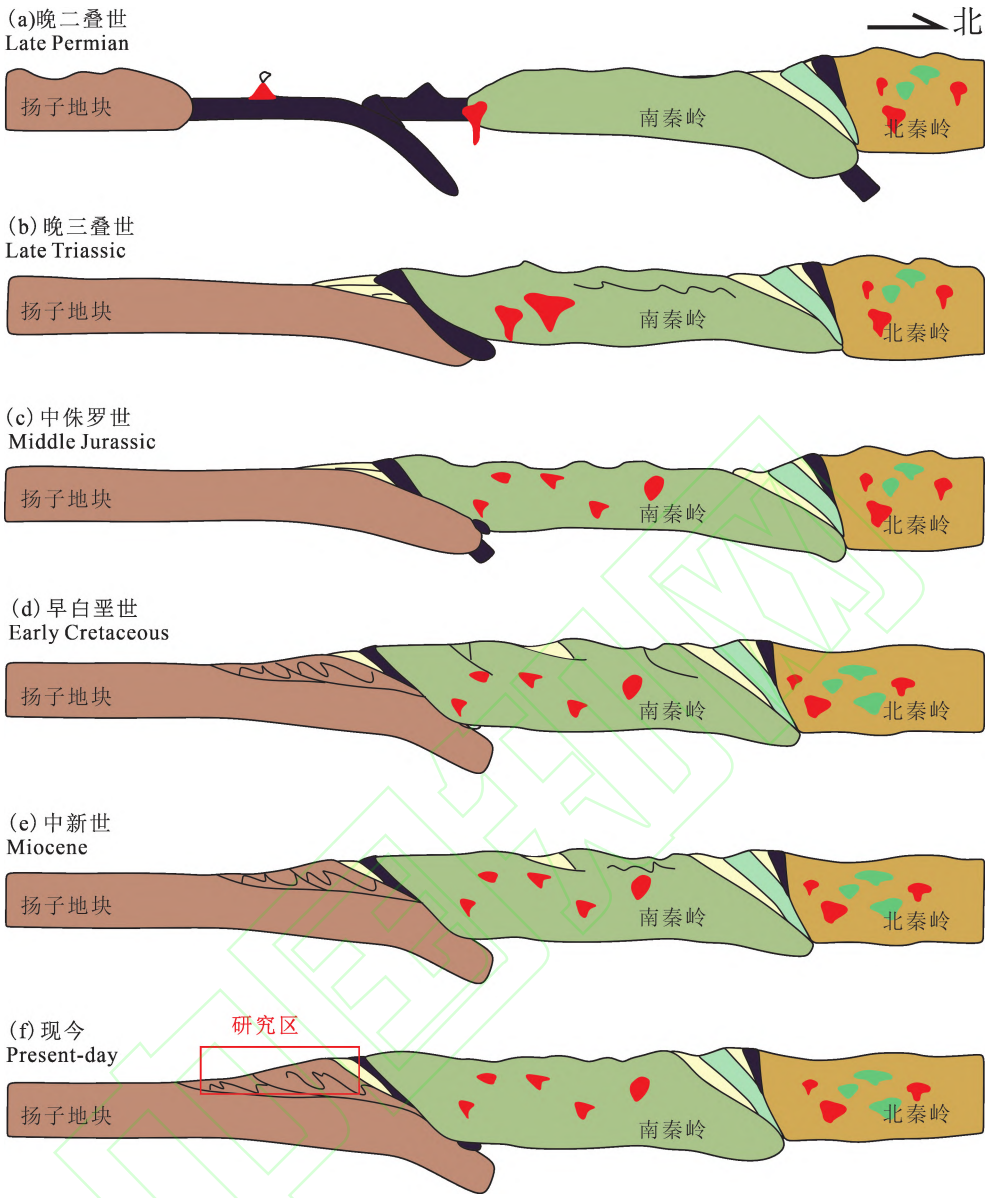

图 8 米仓山隆起中生代以来构造演化过程图(据 Dong Yunpeng et al.,2021,2022 修改)

Fig. 8 Tectonic evolutionary process diagram of the Micang Mountain uplift since the Mesozoic (modified after Dong Yunpeng et al.,2021, 2022)

成前陆褶皱逆冲带。晚白垩世,秦岭造山带陆内造山作用显著减弱,进入后造山调整阶段,构造活动强度随之降低(Liu Shaofeng et al., 2001; Xu ChangHai et al.,2010; Yang Zhao et al.,2013; Qian Tao et al.,2023)。此时,大西洋和印度洋持续扩张导致欧亚板块形成低缓夷平面,研究区进入短暂的构造停滞期,冷却和剥蚀可忽略不计(Yang Zhao et al.,2013; 罗良等, 2015; 张建勇等, 2024; Tong Kui et al.,2025)。同时,太平洋板块俯冲向东后撤,由于俯冲方式的改变和板块运动速率的降低,区域应力场由挤压-走滑转为拉张-走滑,太平洋俯冲对研究区的影响大幅减弱,进一步抑制了研究区隆升和剥蚀作用(图 8e; Northrup et al.,1995; Chen Hong et al, 2015; Shi Hongcai et al.,2016; Valer'evna 等, 2017)。该阶段地层温度从早白垩世末的 70℃仅缓慢降至中新世的 50~60℃,与构造活动的显著减弱形成直接对应关系。

5.1.5 构造叠加和整体隆升(中新世至今)

中新世(20 Ma)以来,米仓山地区进入末次快速隆升阶段,受到新生代全球构造格局的重组控制。印度板块在近 SN 向转换断层的控制下快速向北漂移与欧亚板块发生陆-陆碰撞,青藏高原的持续隆升及其向东的远程构造效应成为区域主导动力(张国伟等, 1995; Hu Shengbiao et al.,2006; 何登发等,

2011；Valer'evna 等，2017；李永东等，2022）。受青藏高原持续隆升远程效应控制，米仓山地区及毗邻盆地整体呈现由西向东逐步隆升的特征（胡圣标等，2005；常远等，2010；Dong Yunpeng et al.，2011；Yang Zhao et al.，2017）。在继承晚白垩世沉格局的基础上，原有构造被新生代断层激活，米仓山地区快速隆升，地层温度自晚白垩世-中新世的稳定期（约 50～60℃）骤降至地表温度（20℃），冷却速率约为 1.5℃/Ma，且逐步发育形成以复合叠加构造为主的构造样式，至此米仓山地区的构造形态已基本定型（图 8f；张茜，2010；孙东，2012；Yang Zhao et al.，2013，2017；朱晨曦，2023）。

综上所述，米仓山隆起多阶段隆升-剥蚀过程呈现出“多幕式”构造变形特征：早中生代碰撞造山奠定构造基底，中-晚中生代陆内变形形成主体构造格局，新生代叠加改造完成最终定型，中生代（印支期-燕山期）隆升主要受控于扬子地块-秦岭地块陆内汇聚，新生代（喜马拉雅期）隆升主要受到印度板块对欧亚大陆板块的挤压驱动（Xu Changhai et al.，2010；孙东，2012；李永东等，2022；张建勇等，2024；Tong Kui et al.，2025）。

5.2 中生代地层物源分析对隆升过程的约束

5.2.1 上三叠统须家河组物源分析

上三叠统须家河组的碎屑锆石 U-Pb 年龄谱图与物源区对比分析表明（图 5，图 6），古元古代早期-古元古代晚期（～2460 Ma 和～1870 Ma）的锆石特征与华北克拉通南缘基底岩石的年代格架高度吻合，表示该区域是此年龄峰值最主要的物源供给区，部分锆石物源来自扬子地块北缘（Luo Liang et al.，2014；Zhang Yong et al.，2015；Shao Tongbin et al.，2016；张勇，2016；李双建等，2018）。新元古代（～806 Ma）锆石与 Rodinia 超大陆裂解有关系（Li Zhengxiang et al.，2008），其可能存在南秦岭造山带、扬子地块北缘、龙门山褶皱带和松潘-甘孜多个潜在物源区（Shi Yu et al.，2013；Wang Lijuan et al.，2013；Luo Liang et al.，2014；Zhang Yong et al.，2015；张勇，2016；李双建等，2018）。川西北剑阁等地可能受到部分龙门山造山带和卷入龙门山褶皱冲断带的部分松潘-甘孜物源区的影响，川北至川东北地区则主要受南秦岭造山带和扬子地块北缘物源区的影响（李瑞保等，2010；杨映涛等，2013；Zhang Yong et al.，2015；Shao Tongbin et al.，2016；张勇，2016；Zhu Min et al.，2017）。古生代（～457 Ma）锆石年龄与加里东造山运动在时间上相关联，其物源区主要为北秦岭造山带，南秦岭造山带也提供部分物源（Luo Liang et al.，2014；Zhang Yong et al.，2015；Shao Tongbin et al.，2016）。最年轻的中生代峰值（～230 Ma）锆石，因秦岭造山带和龙门山造山带隆起，阻挡了华北克拉通和松潘-甘孜的物源供给，南秦岭大面积出露的 240～210 Ma 年龄范围的岩浆岩很可能是物源区（Luo Liang et al.，2014；李双建等，2018）。

须家河组沉积形成时，正值华北板块和扬子地块碰撞及秦岭造山带隆起时期，因此华北克拉通南缘和南秦岭是此时的主要物源区，扬子地块北缘、龙门山造山带和松潘甘孜褶皱带提供的物源有限（图 9a）。甚至有研究认为松潘甘孜地区在 200 Ma 的时候仍处于持续沉积状态，须家河组沉积序列不可能来源于同期正在沉积的序列，因此不为研究区提供物源（Bruguier et al.，1997；Zhang Hongfei et al.，2006；Luo Liang et al.，2014；张勇，2016）。但沉积相分析显示在须家河组沉积中晚期，扬子地块北缘米仓山地区已经成为须家河组沉积的主要物源区（林良彪等，2006；张茜，2010；Luo Liang et al.，2013；闫心宇等，2025）。

5.2.2 下侏罗统白田坝组物源分析

下侏罗统白田坝组中碎屑锆石 U-Pb 年龄谱图与物源区对比分析可知（图 5，图 7），古元古代早期-古元古代晚期到（～2481 Ma 和～1849 Ma）的锆石，理论上华北地块南部可作为重要物源（Cui Minli et al.，2011；Shi Yu et al.，2013；Qian Tao et al.，2023），但中-晚三叠世造山作用形成的秦岭造山带的高地形阻隔了源自华北的碎屑向南秦岭南翼输送，华北克拉通的碎屑无法直接到达米仓山南缘，该年龄的碎屑锆石主要是沉积再旋回带来的（张勇，2016；Qian Tao et al.，2023）。新元古代晚期（～801 Ma）锆石年龄的物源主要对应南秦岭北大巴山地区、扬子地块北缘、松潘甘孜地区和龙门山褶皱带地区（Li Yingqiang et al.，2016；Qian Tao et al.，2023）。早古生代（～448 Ma）锆石年龄与加里东造山运动在时间上相关联，其物源区主要为北秦岭造山带，南秦岭造山带也提供部分物源。最年轻的峰值（～214 Ma）锆石年龄峰值与秦岭-大别山造山带三叠纪陆内俯冲碰撞时间一致，可能主要来源于南秦岭（Shi Yu et al.，2013；李双建等，2018；Liu Songnan et al.，2021）。

与上三叠统须家河组对比发现，下侏罗统白田坝组中-新元古代的锆石明显增多，来自南秦岭地块

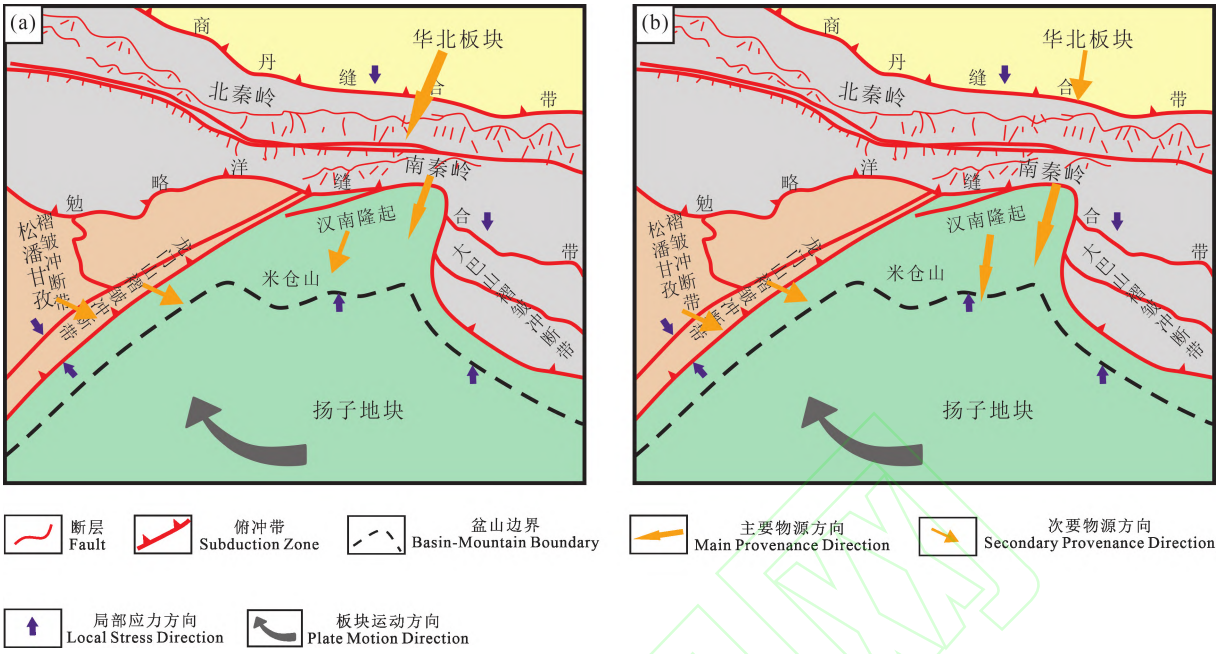

图 9 四川盆地北部晚三叠世-早侏罗世物源供给变化

Fig. 9 Variations in provenance supply in the northern Sichuan basin from the Late Triassic to Early Jurassic

(a)—上三叠统须家河组物源;(b)—下侏罗统白田坝组物源

(a)—provenance of the Upper Triassic Xujiahe Formation; (b)—provenance of the Lower Jurassic Baitianba Formation

和扬子地块北缘的碎屑锆石成为第一物源区,而新太古代到中元古代晚期的碎屑锆石减少,表明从接收的来自华北克拉通南缘的碎屑锆石减少,由于秦岭造山带的持续隆升,阻挡了大量华北克拉通的碎屑物质南下提供物源,因此下侏罗统白田坝组的主要沉积物源区为上扬子地块北缘和南秦岭地区(图9b)。

5.2.3 物源贡献差异对初次隆升时间的约束

扬子地块与华北板块自中三叠世晚期开始碰撞,南秦岭造山带开始隆升,汉南-米仓山地区随后依次隆升,为周围低势区提供物源(Dong Yunpeng et al.,2021)。晚三叠世到早侏罗世地层沉积过程中,新元古代的锆石主要来源于南秦岭及上扬子地块北缘。随着地层沉积,南秦岭虽仍保持物源供给,但此时期的碎屑锆石数量明显增多,表明米仓山地区物源贡献逐渐增强。这一变化源于两方面因素:一是米仓山地区作为近源物源区,隆升使得物源供更为直接(李双建等, 2018);二是汉南-米仓山的隆起,会在一定程度上阻挡南秦岭对米仓山南缘地区物源供给。

从晚三叠世到早侏罗世地层中,米仓山地区供给的新元古代的锆石的占比逐渐增加,物源贡献的变化间接表明米仓山地区在晚三叠世已经隆升,但此时尚未大规模隆升出露地表,到晚三叠世晚期进一步抬升至地表,为晚三叠世中晚期须家河组和早侏罗世白田坝组提供大量物源。物源分析与前文通过低温热年代学得出的在晚三叠世已经开始隆升的研究结论一致。此外,前人研究也指出下侏罗统与中-晚侏罗统的碎屑锆石存在显著差异(李瑞保等,2010; Zhu Xiaoqing et al.,2014; Shao Tongbin et al.,2016; Qian Tao et al.,2023),这种差异主要源于从印支期到燕山期的造山旋回变化,以及盆地从周缘前陆盆地到陆内凹陷的演化转变(Shao Tongbin et al.,2016),与米仓山隆起的隆升速率的阶段性变化也有一定的关系。

6 结论

(1)本文根据低温热年代学系统的重建了米仓山南缘中生代以来的多阶段隆升-剥蚀演化过程:受扬子地块向秦岭地块俯冲作用影响,米仓山南缘从晚三叠世(约 230 Ma)已开始缓慢隆升,抬升冷却速率约为 0.57 ℃/Ma;随着板块俯冲速率的增加,晚侏罗世(约 160 Ma)开始快速隆升剥蚀,抬升冷却速率高达 3.25 ℃/Ma;晚白垩世(约 120 Ma)由于造山作用减弱,隆升速率显著降低,地层温度发生显著变化,冷却速率为 0.2 ℃/Ma;直到中新世(约 20 Ma),受到青藏高原隆升的远程效应向东传递效应影响,米仓山地区再次发生快速隆升,抬升冷却速率

约为 1.5 ℃/Ma。

(2)各阶段冷却速率差异表明,米仓山隆升-剥蚀强度随板块构造作用变化而波动,前期主要受扬子-秦岭地块俯冲控制,晚期则受青藏高原远程构造效应影响,反映出区域构造活动的阶段性增强与减弱。

(3)上三叠统须家河组至下侏罗统白田坝组沉积记录显示,上扬子板块物源贡献比例的渐进式增加,其变化与源区热年代学所揭示的早期缓慢抬升过程高度一致。源区隆升-剥蚀过程与沉积区年代学特征的同步性,直接印证米仓山地区自晚三叠世起已开始构造抬升。

References

Berkana W, Wu Hui, Ling Wenli, Kusky T, Ding Xiaoying. 2022. Neoproterozoic metavolcanic suites in the Micangshan terrane and their implications for the tectonic evolution of the NW Yangtze block, South China. Precambrian Research, 368: 106476.

Bruguier O, Lancelot J R, Malavieille J. 1997. U-Pb dating on single detrital zircon grains from the Triassic Songpan-Ganze flysch (Central China): Provenance and tectonic correlations. Earth and Planetary Science Letters, 152(1): 217～231.

Carter A, Moss S J. 1999. Combined detrital-zircon fission-track and U-Pb dating: A new approach to understanding hinterland evolution. Geology, 27(3): 235～238.

Chang Yuan, Xu Changhai, Reiners P W, Zhou Zuyi. 2010. The exhumation evolution of the Micang Shan-Hannan uplift since Crelaceous: Evidenee from apatite (U-Th)/He dating. Chinese Journal of Geophysics, 53(4): 912～919 (in Chinese with English abstract).

Chen Hong, Hu Jianmin, Wu Guoli, Shi Wei, Geng Yingying, Qu Hongjie. 2015. Apatite fission-track thermochronological constraints on the pattern of late Mesozoic-Cenozoic uplift and exhumation of the Qinling Orogen, central China. Journal of Asian Earth Sciences, 114: 649～673.

Chen Qiong, Sun Min, Long Xiaoping, Zhao Guochun, Yuan Chao. 2016. U-Pb ages and Hf isotopic record of zircons from the late Neoproterozoic and Silurian-Devonian sedimentary rocks of the western Yangtze block: Implications for its tectonic evolution and continental affinity. Gondwana Research, 31: 184～199.

Chen Zhuxin, Jia Dong, Wei Guoqi, Li Benliang, Lei Yongliang. 2008. Meso-Cenozoic sediment transport and tectonic transition in the western Sichuan foreland basin. Geology in China, (3): 472～481 (in Chinese with English abstract).

Chen Zhuxin, Li Wei, Wang Lining, Lei Yongliang, Yang Guang, Zhang Benjian, Yin Hong, Yuan Baoguo. 2019. Structural geology and favorable exploration prospect belts in northwestern Sichuan basin, SW China. Petroleum Exploration and Development, 46(2): 397～408 (in Chinese with English abstract).

Cogné N, Chew D M, Donelick R A, Donelick R A, Ansberque C. 2020. LA-ICP-MS apatite fission track dating: A practical zeta-based approach. Chemical Geology, 531: 119302.

Condon D, Zhu Maoyan, Bowring S l, Wang Wei, Yang Aihua, Jin Yugan. 2005. U-Pb Ages from the Neoproterozoic Doushantuo Formation, China. Science, 308(5718): 95～98.

Cui Minli, Zhang Baolin, Zhang Lianchang. 2011. U-Pb dating of baddeleyite and zircon from the Shizhaigou diorite in the southern margin of North China Craton: Constrains on the timing and tectonic setting of the Paleoproterozoic Xiong'er Group. Gondwana Research, 20(1): 184～193.

Deng Bin, Shigeru S, Liu Shugen, Li Zhiwu, Li Jinxi. 2014. Wedge-thrust folding in the Micangshan constrained by low-temperature thermochronometer model and its significance. Chinese Journal of Geophysics, 57(4): 1155～1168 (in Chinese with English abstract).

Donelick R A, O'sullivan P B, Ketcham R A. 2005. Apatite fission-track analysis. Reviews in Mineralogy and Geochemistry, 58(1): 49～94.

Dong Yunpeng, Zhang Guowei, Neubauer F, Liu Xiaoming, Genser J, Hauzenberger C. 2011. Tectonic evolution of the Qinling orogen, China: Review and synthesis. Journal of Asian Earth Sciences, 41(3): 213～237.

Dong Yunpeng, Liu Xiaoming, Santosh M, Chen Qing, Zhang Xiaoning, Li Wei, He Dengfeng, Zhang Guowei. 2012. Neoproterozoic accretionary tectonics along the northwestern margin of the Yangtze block, China: Constraints from zircon U-Pb geochronology and geochemistry. Precambrian Research, 196～197: 247～274.

Dong Yunpeng, Sun Shengsi, Santosh M, Zhao Jie, Sun Jiaopeng, He Dengfeng, Shi Xiaohui, Hui Bo, Cheng Chao, Zhang Guowei. 2021. Central China Orogenic Belt and amalgamation of East Asian continents. Gondwana Research, 100: 131～194.

Dong Yunpeng, Shi Xiaohui, Sun Shengsi, Sun Jiaopeng, Hui Bo, He Dengfeng, Chong Fubao, Yang Zhao. 2022. Co-evolution of the Cenozoic tectonics, geomorphology, environment and ecosystem in the Qinling Mountains and adjacent areas, Central China. Geosystems and Geoenvironment, 1(2): 100032.

Dong Yunpeng, Hui Bo, Sun Shengsi, Yang Zhao, Zhang Feifei, He Dengfeng, Sun Jiaopeng, Shi Xiaohui. 2022. Multiple orogeny and geodynamics from Proto- Tethys to Paleo- Tethys of the Central China Orogenic Belt. Acta Geologica Sinica, 96(10): 3426～3448(in Chinese with English abstract).

Duan Liang, Meng Qingren, Zhang Chengli, Liu Xiaoming. 2011. Tracing the position of the South China block in Gondwana: U-Pb ages and Hf isotopes of Devonian detrital zircons. Gondwana Research, 19(1): 141～149.

Fang Xinyan, Geng Ansong, Liang Xiao, Cheng Bin, Li Yun, Jiang Wenmin, Wu Liangliang. 2022. Comparison of the Ediacaran and Cambrian petroleum systems in the Tianjingshan and the Micangshan uplifts, northern Sichuan basin, China. Marine and Petroleum Geology, 145: 105876.

Fitzgerald P G, Malusà M G. 2019. Concept of the exhumed partial annealing (retention) zone and age-elevation profiles in thermochronology. In: Malusà M G, Fitzgerald, P G, eds. Fission-Track Thermochronology and its Application to Geology. Chambrigae: Springer International Publishing.

Galbraith R F, Laslett G M. 1993. Statistical models for mixed fission track ages. Nuclear Tracks and Radiation Measurements, 21(4): 459～470.

Gautheron C, Tassan-Got L. 2010. A Monte Carlo approach to diffusion applied to noble gas/helium thermochronology. Chemical Geology, 273(3): 212～224.

Gautheron C, Barbarand J, Ketcham R A, Tassan-Got L, Van Der Beek P, Pagel M, Pinna-Jamme R, Couffignal F, Fialin M. 2013. Chemical influence on α-recoil damage annealing in apatite: Implications for (U-Th)/He dating. Chemical Geology, 351: 257～267.

Gleadow A J W, Duddy I R, Green P F, Hegarty K A. 1986. Fission track lengths in the apatite annealing zone and the interpretation of mixed ages. Earth and Planetary Science Letters, 78(2): 245～254.

Green P F. 1981. A new look at statistics in fission-track dating. Nuclear Tracks, 5(1): 77～86.

Guenthner W R, Reiners P W, Ketcham R A, Nasdala L, Giester G. 2013. Helium diffusion in natural zircon: Radiation damage, anisotropy, and the interpretation of zircon (U-Th)/He thermochronology. American Journal of Science, 313(3): 145～198.

He Dengfa, Li Desheng, Zhang Guowei, Zhao Luzi, Fan Chun, Lu Renqi, Wen Zhu. 2011. Formation and evolution of multi-cycle superposed Sichuan basin, China. Chinese Journal of Geology, 46(3): 589～606 (in Chinese with English abstract).

He Dengfa, Jia Chengzao, Zhao Zhe, Zhao Luzi, Bao Hongping, Gao Shanlin, Lu Guo, Zheng Na, Yang Zhikun, Cheng Changyu. 2025. Vertically interweaving superimposed structures: Distinct features of cratonic basins in China. Acta Geologica Sinica, 99(12): 3999～4018(in Chinese with English abstract).

Hendrix M S, Dumitru T A, Graham S A. 1994. Late Oligocene-early Miocene unroofing in the Chinese Tian Shan: An early effect of the India-Asia collision. Geology, 22(6): 487～490.

Hou Fanghui. 2015. Research on the distribution and tectonic characteristics of the Mesozoic strata of the East China Sea Shelf basin. Doctoral dissertation of Ocean University of China (in Chinese with English abstract).

Hu Shengbiao, Hao Jie, Fu Mingxi, Wu Weiping, Wang Jiyang. 2005. Cenozoic denudation and cooling history of Oinling-Dabie-Sulu orogens: Apatite fission track thermochronology constraints. Acta Petrologica Sinica, (4): 1167～1173 (in Chinese with English abstract).

Hu Shengbiao, Raza A, Min K, Kohn B P, Reiners P W, Ketcham R A, Wang Jiyang, Gleadow A J W. 2006. Late Mesozoic and Cenozoic thermotectonic evolution along a transect from the north China craton through the Qinling orogen into the Yangtze craton, central China. Tectonics, 25(6): 2006TC001985.

Huang Hanyu, He Dengfa, Li Yingqiang, Zhang Chen, Li Di. 2024. Provenance and paleogeography of the Early Paleozoic basin in the northern Yangtze Block: Constraints from detrital zircon U-Pb-Hf data. Gondwana Research, 125: 210～228.

Hui Bo, Dong Yunpeng, Sun Shengsi, Zhang Feifei, Zhu Xin, Tavakoli Neda, Li Yongcheng, Zang Rutao. 2025. Late Mesoproterozoic passive continental margin in the northwestern Yangtze block, South China: Insights from the Huodiya Group in the Hannan-Micangshan Massif. Geological Journal, 60(2): 272～289.

Lai Shaocong, Qin Jiangfeng. 2010. Zircon U-Pb dating and Hf isotopic composition of the diabase dike swarm from Sanchazi area, Mianlue suture: Chronology evidence for the Paleo-Tethys oceanic crust subduction. Journal of Earth Sciences and Environment, 32(1): 27～33.

Lease R O, Burbank D W, Gehrels G E, Wang Zhicai, Yuan Daoyang. 2007. Signatures of mountain building: Detrital zircon U/Pb ages from northeastern Tibet. Geology, 35(3): 239～242.

Li Chenxing, Chang Jian, Qiu Nansheng, Cao Shiji, Zhang Yinglin, Zheng Liqing. 2025. Development and application of in-situ LA-ICP-MS apatite fission track experiment procedure. Acta Geoscientica Sinica, 46(2): 471～482 (in Chinese with English abstract).

Li Hongyan, He Bin, Xu Yigang, Huang Xiaolong. 2010. U-Pb and Hf isotope analyses of detrital zircons from Late Paleozoic sediments: Insights into interactions of the North China Craton with surrounding plates. Journal of Asian Earth Sciences, 39(5): 335～346.

Li Jinxi, Li Zhiwu, Liu Shugen, Sun Dong, Deng Bin. 2015. Paleostress reconstruction of micangshan anticlinorium on the southern margin of the Qinling orogenic belts, China. Acta Geologica Sinica-English Edition, 89(2): 505～518.

Li Ruibao, Pei Xianzhi, Liu Zhanqing, Li Zuochen, Ding Sanping, Liu Zhigang, Zhang Xiaofei, Chen Guochao, Chen Youxin, Zhang Xueliang. 2010. Basin-mountain coupling relationship of foreland basins between Dabashan and Northeastern Sichuan—The evidence from LA-ICP-MS U-Pb dating of the detrital zircons. Acta Geoscientica Sinica, 84(8): 1118～1134 (in Chinese with English abstract).

Li Sanzhong, Zhang Guowei, Zhou Lihong, Zhao Guowei, Liu Xin, Suo Yanhui, Liu Bo, Jin Chong, Dai Liming. 2011. The opposite Meso-Cenozoic intracontinental deformations under the superconvergence: Rifting and extension in the North China Craton and shortening and thrusting in the South China Craton. Earth Science Frontiers, 18(3): 79～107 (in Chinese with English abstract).

Li Shuangjian, Sun Dongsheng, Cai Liguo, Gao Ping, Li Tianyi, Yuan Yusong, Zheng Menglin, Qiu Dengfeng. 2018. Detrital zircon U-Pb geochronology of Micang mountain piedmont zone, northern Sichuan basin and its significance to basin-mountain evolution. Geotectonica et Metallogenia, 42(6): 1087～1107 (in Chinese with English abstract).

Li Yanfeng, Qu Guosheng, Liu Shu, Zhang Hong. 2008. Structural characters and mechanism in the Micang Shan and southern Daba Shan mountains front. Geotectonica et Metallogenia, (3): 285～292 (in Chinese with English abstract).

Li Yingqiang, He Dengfa, Li Di, Wen Zhu, Mei Qinghua, Li Chuanxin, Sun Yanpeng. 2016. Detrital zircon U-Pb geochronology and provenance of Lower Cretaceous sediments: Constraints for the northwestern Sichuan pro-foreland basin. Palaeogeography, Palaeoclimatology, Palaeoecology, 453: 52～72.

Li Yongdong, Xiong Xiong, Feng Yashan. 2022. Mesozoic uplift of the Dabashan and Micangshan-Hannan dome in the South Qinling orogenic belt. Scientia Sinica Terrae, 52(3): 426～436 (in Chinese with English abstract).

Li Zhengxiang, Bogdanova S V, Collins A S, Davidson A, De Waele B, Ernst R E, Fitzsimons I C W, Fuck R A, Gladkochub D P, Jacobs J, Karlstrom K E, Lu S, Natapov L M, Pease V, Pisarevsky S A, Thrane K, Vernikovsky V. 2008. Assembly, configuration, and break-up history of Rodinia: A synthesis. Precambrian Research, 160(1): 179～210.

Lin Liangbiao, Chen Hongde, Cui Changbo, Hu Xiaoqiang, Li Junwen. 2006. Sandstone compositions and paleogeographic evolution of the Upper Triassic Xujiahe Formation in the western Sichuan basin, china. 2006. Petroleum Geology & Experiment, (6), 511～517 (in Chinese with English abstract).

Liu Shaofeng, Guowei Zhang, Dai Shaowu. 2001. Evolution of Qinling Mianlue belt: Evidence from sedimentology and tectonics of the northern Yangtze, China. Gondwana Research, 4(4): 690～691.

Liu Songnan, Wang Yu, Ma Huimin, Qian Tao. 2021. Timing and nature of intracontinental deformation at the northwestern margin of the Sichuan basin, China: Evidence from structural analysis and detrital zircon U-Pb ages. Geological Magazine, 158(8): 1504～1526.

Liu Xiang, Zhan Qingyao, Zhu Dicheng, Wang Qing, Xie Jincheng, Zhang Langlang. 2021. Provenance and tectonic uplift of the Upper Triassic strata in the southern Songpan-Ganzi fold belt, SW China: Evidence from detrital zircon geochronology and Hf isotope. Acta Petrologica Sinica, 37(11): 3513～3526 (in Chinese with English abstract).

Luo Liang, Jia Dong, Qi Jiafu, Wei Guoqi, Deng Fei. 2013. Tectono-sedimentary Evolution of the Late Triassic Xujiahe Formation in the Sichuan basin. Acta Geologica Sinica-English Edition, 87(6): 1554～1568.

Luo Liang, Qi Jiafu, Zhang Mingzheng, Wang Kai, Han Yuzhen. 2014. Detrital zircon U-Pb ages of Late Triassic-Late Jurassic deposits in the western and northern Sichuan basin margin: Constraints on the foreland basin provenance and tectonic implications. International Journal of Earth Sciences, 103(6): 1553～1568.

Luo Liang, Qi Jiafu, Zhang Mingzheng. 2015. Difference study on evolution and deformation of the fold-thrust belts surrounding Sichuan basin. Geological Review, 61(3): 525～535 (in Chinese with English abstract).

Ma Qianli, Yang Jianghai, Du Yuansheng, Dai Xianduo, Chai Rong, Guo Hua, Xu Yajun. 2021. Early Triassic initial collision between the North China and South China blocks in the eastern Qinling Orogenic Belt. Tectonophysics, 814: 228965.

Meng Qingren, Zhang Guowei. 1999. Timing of collision of the North and South China blocks: Controversy and reconciliation. Geology, 27(2): 123～126.

Meng Qingren, Wang E, Hu Jianmin. 2005. Mesozoic sedimentary evolution of the northwest Sichuan basin: Implication for continued clockwise rotation of the South China block. Bulletin of Geological Society of America, 117(3～4): 396～410.

Northrup C J, Royden L H, Burchfiel B C. 1995. Motion of the Pacific plate relative to Eurasia and its potential relation to Cenozoic extension along the eastern margin of Eurasia. Geology, 23(8): 719～722.

Peng Heng, Wang Jianqiang, Zattin M, Liu Chiyang, Han Peng, Zhang Shaohua. 2018. Late Triassic-early jurassic uplifting in eastern Qilian Mountain and its geological significance: Evidence from apatite fission track thermochronology. Earth Science, 43(6): 1983～1996 (in Chinese with English abstract).

Peng Liyong. 2023. The sub-surface structural character and evolution mechanism of Micang Mountain-Zhenba zone. Master's thesis of China University of Geosciences (Beijing) (in Chinese with English abstract).

Qian Tao, Li Wangpeng, Liu Shaofeng. 2023. Early to Middle Jurassic sedimentation within the northern Sichuan basin in response to exhumation of the South Qinling orogenic belt, central China. Palaeogeography, Palaeoclimatology, Palaeoecology, 630: 111805.

Qiu Nansheng, Wang Jiyang, Mei Qinghua, Jiang Guang, Tao Cheng. 2010. Constraints of (U-Th)/He ages on early Paleozoic tectonothermal evolution of the Tarim basin, China. Scientia Sinica Terrae, 53: 964 ～ 976 (in Chinese with English abstract).

Qiu Nansheng, He Lijuan, Chang Jian, Zhu Chuanqing. 2020. Research progress and challenges of thermal history reconstruction in sedimentary basins. Petroleum Geology & Experimen, 42(5): 790 ～ 802 (in Chinese with English abstract).

Reiners P W, Zhou Zuyi, Ehlers T A, Xu Changhai, Brandon M T, Donelick R A, Nicolescu S. 2003. Post-orogenic evolution of the Dabie Shan, eastern China, from (U-Th)/He and fission-track thermochronology. American Journal of Science, 303(6): 489～518.

Shao Tongbin, Cheng Nanfei, Song Maoshuang. 2016. Provenance and tectonic-paleogeographic evolution: Constraints from detrital zircon U-Pb ages of Late Triassic-Early Jurassic deposits in the northern Sichuan basin, central China. Journal of Asian Earth Sciences, 127: 12～31.

Shi Hongcai, Shi Xiaobin, Glasmacher U A, Yang Xiaoqiu, Stockli D F. 2016. The evolution of eastern Sichuan basin, Yangtze block since Cretaceous: Constraints from low temperature thermochronology. Journal of Asian Earth Sciences, 116: 208～221.

Shi Yu, Yu Jin Hai, Santosh M. 2013. Tectonic evolution of the Qinling orogenic belt, Central China: New evidence from geochemical, zircon U-Pb geochronology and Hf isotopes. Precambrian Research, 231: 19～60.

Sircombe K N. 1999. Tracing provenance through the isotope ages of littoral and sedimentary detrital zircon, eastern Australia. Sedimentary Geology, 124(1): 47～67.

Sun Dong. 2012. The structural character and Meso-Cenozoic evolution of Micang Mountain structural zone, northern Sichuan basin, China. Doctoral dissertation of Chengdu University of Technology (in Chinese with English abstract).

Taylor J P, Fitzgerald P G. 2011. Low-temperature thermal history and landscape development of the eastern Adirondack Mountains, New York: Constraints from apatite fission-track thermochronology and apatite (U-Th)/He dating. Geological Society of America Bulletin, 123(3～4): 412～426.

Tian Tao, Yang Peng, Yao Jianming, Duan Zhonghui, Ren Zhanli, Fu Deliang, Yang Fu. 2021. New detrital apatite fission track thermochronological constraints on the Meso-Cenozoic tectono-thermal evolution of the Micangshan-Dabashan tectonic Belt, central China. Frontiers in Earth Science, 9: 754137.

Tian Yuntao, Zhu Chuanqing, Xu Ming, Rao Song, Barry P K, Hu Shengbiao. 2010. Exhumation history of the Micangshan-Hannan dome since cretaceous and its tectonic significance: Evidences from apatite fission track analysis. Chinese Journal of Geophysics, 53(4): 920 ～ 930 (in Chinese with English abstract).

Tian Yuntao, Kohn B P, Zhu Chuanqing, Xu Ming, Hu Shengbiao, Gleadow A J W. 2012. Post - orogenic evolution of the Mesozoic Micang Shan foreland basin system, central China. Basin Research, 24(1): 70～90.

Tian Yuntao, Yuan Yusong, Hu Shengbiao, Qiu Nansheng. 2017. Application of low-temperature thermochronology to sedimentary basins: case studies in the northern Sichuan basin. Earth Science Frontiers, 24(3): 105～115 (in Chinese with English abstract).

Tong Kui, Li Zhiwu, Liu Shugen, Li Jinxi, Sun Dong, Deng Bin, Wu Wenhui, Ye Yuehao, Wang Zijian, Jiang Xun, Li Yin, Sun Xiao. 2025. Episodic cooling of the Hannan-Micangshan Dome at the northern margin of the Yangtze Block, Central China: Response to progressive convergence in the eastern Tethys since the Mesozoic. Journal of Asian Earth Sciences, 278: 106409.

Valer'evna D L, Wang Pengcheng, Li Sanzhong, Cao Xianzhi, Zhou Zaizheng, Hu Mengying, Suo Yanhui, Guo Lingli, Wang Yongming, Li Xiyao, Liu Xin, Yu Shenyao. 2017. Meso-cenozoic evolution of earth surface system under the east Asian tectonic superconvergence. Marine Geology & Quaternary Geology, 37(4): 33～64 (in Chinese with English abstract).

Wang Anqi, Yang Debin, Yang Haotian, Mu Maosong, Quan Yikang, Hao Leran, Xu Wenliang. 2021. Detrital zircon geochronology and provenance of sediments within the Mesozoic basins: New insights into tectonic evolution of the Qinling Orogen. Geoscience Frontiers, 12(3): 101107.

Wang Lijuan, Griffin W L, Yu Jinhai, O'Reilly S Y. 2013. U-Pb and Lu-Hf isotopes in detrital zircon from Neoproterozoic sedimentary rocks in the northern Yangtze block: Implications for Precambrian crustal evolution. Gondwana Research, 23(4): 1261～1272.

Wang Qihang. 2025. Quantitative deformation reconstruction of the peripheral Sichuan basin since Mesozoic. Master's thesis of China University of Geosciences (Beijing) (in Chinese with English abstract).

Weislogel A L, Graham S A, Chang E Z, Wooden J L, Gehrels G E, Yang Hengshu. 2006. Detrital zircon provenance of the Late Triassic Songpan-Ganzi complex: Sedimentary record of collision of the North and South China blocks. Geology, 34(2): 97～100.

Wolf R A, Farley K A, Silver L T. 1996. Helium diffusion and low-temperature thermochronometry of apatite. Geochimica et Cosmochimica Acta, 60(21): 4231～4240.

Wu Yuanbao, Zheng Yongfei. 2013. Tectonic evolution of a composite collision orogen: An overview on the Qinling-Tongbai-Hong'an-Dabie-Sulu orogenic belt in central China. Gondwana Research, 23(4): 1402～1428.

Xu ChangHai, Zhou ZuYi, Chang Yuan, Guillot F. 2010. Genesis of Daba arcuate structural belt related to adjacent basement upheavals: Constraints from Fission-track and (U-Th)/He thermochronology. Science China Earth Sciences, 53(11): 1634～1646.

Xu Huaming, Liu Shu, Qu Guosheng, Li Yanfeng, Sun Gang, Liu Kang. 2009. Structural Characteristics and Formation Mechanism in the Micangshan Foreland, South China. Acta Geologica Sinica-English Edition, 83(1): 81～91.

Xu Jun, Fu Qiang, Yang Wentao. 2024. Detrital zircon U-Pb age signatures and response to surrounding orogens of the North China basin in the Late Paleozoic. Journal of Henan Polytechnic University (Natural Science): 1～15 (in Chinese with English abstract).

Xu Xianbing, Tang Shuai, Lin Shoufa. 2016. Detrital provenance of Early Mesozoic basins in the Jiangnan domain, South China: Paleogeographic and geodynamic implications. Tectonophysics, 675: 141～158.

Yamada R, Murakami M, Tagami T. 2007. Statistical modelling of annealing kinetics of fission tracks in zircon: Reassessment of laboratory experiments. Chemical Geology, 236(1～2): 75～91.

Yan Xinyu, Liu Lei, Wang Xiaojuan, Zhu Shuyue, Zhao Fei, Zheng Chao, Ma Xiancheng, Zhang Rui. 2025. Basin-Orogen coupling processes and paleogeographic evolution of the Late Triassic, northwest of Sichuan basin. Journal of Chengdu University of Technology(Science & Technology Edition) (in Chinese with English abstract).

Yan Yi, Lin Ge, Wang Yuejun, Guo Feng. 2002. The indication of continental detrital sediment to tectonic setting. Advances in Earth Science: 85～90 (in Chinese with English abstract).

Yang Yingtao, Fu Ju, Wu Ling, Meng Xin. 2013. Provenance analysis of the second and forth member of Xujiahe Formation in the middle part of western Sichuan depression. Petroleum Geology and Engineering, 27(6): 26～29+148～149 (in Chinese with English abstract).

Yang Zhao, Ratschbacher, Jonckheere R, Enkelmann E, Dong Yunpeng, Shen Chuanbo, Wiesinger M, Zhang Qian. 2013. Late-stage foreland growth of China's largest orogens (Qinling, Tibet): Evidence from the Hannan-Micang crystalline massifs and the northern Sichuan basin, central China. Lithosphere, 5(4): 420～437.

Yang Zhao, Shen Chuanbo, Ratschbacher L, Enkelmann E, Jonckheere R, Wauschkuhn B, Dong Yunpeng. 2017. Sichuan basin and beyond: Eastward foreland growth of the Tibetan Plateau from an integration of Late Cretaceous - Cenozoic fission track and (U - Th)/He ages of the eastern Tibetan Plateau, Qinling, and Daba Shan. Journal of Geophysical Research: Solid Earth, 122(6): 4712～4740.

Zhang Guowei, Meng Qingren, Lai Shaocong. 1995. Structural features of the Qinling-Dabie orogenic belt. Science in China (Series B), 38: 994～1003 (in Chinese with English abstract).

Zhang Guowei, Dong Yunpeng, Lai Shaocong, Guo Anlin, Meng Qingren, Liu Shaofeng, Cheng Shunyou, Yao Anping, Zhang Zongqing, Pei Xianzhi, Li Sanzhong. 2003. Mianlue tectonic zone and Mianlue suture zone on southern margin of Qinling Dabie orogenic belt. Science in China (series D), 33(12): 1121～1135 (in Chinese with English abstract).

Zhang Guowei, Cheng Shunyou, Guo Anlin, Dong Yunpeng, Lai Shaocong, Yao Anping. 2004. Mianlue paleo-suture on the southern margin of the Central Orogenic System in Qinling-Dabie-with a discussion of the assembly of the main part of the continent of China. Geological Bulletin of China, (Z2): 846～853 (in Chinese with English abstract).

Zhang Hongfei, Zhang Li, Harris N, Jin Lan Lan, Yuan Honglin. 2006. U-Pb zircon ages, geochemical and isotopic compositions of granitoids in Songpan-Garze fold belt, eastern Tibetan Plateau: constraints on petrogenesis and tectonic evolution of the basement. Contributions to Mineralogy and Petrology, 152(1): 75～88.

Zhang Jianyong, Chang Jian, Li Wenzheng, Fu Xiaodong, Yang Lei, He Yuan. 2024. Tectono-thermal evolution of the Micangshan uplift in the northern Sichuan basin. Sedimentary Geology and Tethyan Geology, 44(1): 58～70 (in Chinese with English abstract).

Zhang Kaijun. 1997. North and South China collision along the eastern and southern North China margins. Tectonophysics, 270(1-2): 145～156.

Zhang Qian. 2010. Sedimentary evidences constrain on the uplift of the Micang Shan. Master's thesis of Northwest University (in Chinese with English abstract).

Zhang Wenjun, Qin Xuqian, Gao Tangjun, He Hongbing. 2016. Characteristics and evolution of middle Cenozoic tectonics, Micangshan uplift belt. Natural Gas Technology and Economy, 10(2): 22～25, 33, 82 (in Chinese with English abstract).

Zhang Yong. 2016. The provenance of the Xujiahe Formation in the Sichuan basin and remganetization of the hydrocarbon bearing strata in Yangtze block. Doctoral dissertation of Nanjing University (in Chinese with English abstract).

Zhang Yong, Jia Dong, Shen Li, Yin Hongwei, Chen Zhuxin, Li Haibin, Li Zhigang, Sun Chuang. 2015. Provenance of detrital zircons in the Late Triassic Sichuan foreland basin: constraints on the evolution of the Qinling Orogen and Longmen Shan thrust-fold belt in central China. International Geology Review, 57(14): 1806～1824.

Zhang Yueqiao, Dong Shuwen, Wang Haiyan, Feng Mei, Thybo H, Li Jianhua, Gao Rui, Shi Wei. 2022. Coupled lithospheric deformation in the Qinling orogen, central China: Insights from seismic reflection and surface-wave tomography. Geophysical Research Letters, 49(14): e2022GL097760.

Zhao Junhong, Zhou Meifu. 2009. Secular evolution of the Neoproterozoic lithospheric mantle underneath the northern margin of the Yangtze Block, South China. Lithos, 107(3～4): 152～168.

Zheng Binsong, Mou Chuanlong, Wang Xiuping, Chen Hongde. 2021. U-Pb ages, trace elements and Hf isotopes of detrital zircons from the late Permian-early Triassic sedimentary succession in the northern Yangtze Block, South China: Implications for the reconstruction of the South China Block in Pangea. Journal of Asian Earth Sciences, 206: 104609.

Zhu Chenxi. 2023. Research on structural deformation and evolution of the Micang Shan-Daba Shan thrust belt. Master's thesis of China University of Petroleum (Beijing) (in Chinese with English abstract).

Zhu Min, Chen Hanlin, Zhou Jing, Yang Shufeng. 2017. Provenance change from the Middle to Late Triassic of the southwestern Sichuan basin, Southwest China: Constraints from the sedimentary record and its tectonic significance. Tectonophysics, 700～701: 92～107.

Zhu Xiaoqing, Zhu Wenbin, Ge Rongfeng, Wang Xi. 2014. Late Paleozoic provenance shift in the south-central North China craton: Implications for tectonic evolution and crustal growth. Gondwana Research, 25(1): 383～400.

参 考 文 献

Valer'evna D L,王鹏程, 李三忠, 曹现志, 周在征, 胡梦颖, 索艳慧, 郭玲莉, 王永明, 李玺瑶, 刘鑫, 于胜尧. 2017. 东亚大汇聚与中-新生代地球表层系统演变. 海洋地质与第四纪地质, 37(4): 33～64.

常远, 许长海, Reiners W P, 周祖翼. 2010. 米仓山-汉南隆起白垩纪以来的剥露作用:磷灰石(U-Th)/He 年龄记录. 地球物理学报, 53(4): 912～919.

陈竹新, 贾东, 魏国齐, 李本亮, 雷永良. 2008. 川西前陆盆地中-新生代沉积迁移与构造转换. 中国地质, (3): 472～481.

陈竹新, 李伟, 王丽宁, 雷永良, 杨光, 张本健, 尹宏, 苑保国. 2019. 川西北地区构造地质结构与深层勘探层系分区. 石油勘探与开发, 46(2): 397～408.

邓宾, Sueoka S, 刘树根, 李智武, 李金玺. 2014. 米仓山楔入冲断构造模型低温热年代学证据及其意义. 地球物理学报, 57(4): 1155～1168.

董云鹏,惠博,孙圣思,杨钊,张菲菲,何登峰,孙娇鹏,史小辉. 2022. 中国中央造山系原-古特提斯多阶段复合造山过程. 地质学报, 96(10):3426～3448.

何登发, 李德生, 张国伟, 赵路子, 樊春, 鲁人齐, 文竹. 2011. 四川多旋回叠合盆地的形成与演化. 地质科学, 46(3): 589～606.

何登发,贾承造,赵喆,赵路子,包洪平,高山林,鲁国,郑娜,杨志坤,成昌宇. 2025. 垂向交织叠加结构:中国克拉通盆地的重要特色. 地质学报,99(12):3999～4018.

侯方辉. 2015. 东海陆架盆地南部中生代地层分布及构造特征研

究. 中国海洋大学博士学位论文.
胡圣标, 郝杰, 付明希, 吴维平, 汪集旸. 2005. 秦岭-大别-苏鲁造山带白垩纪以来的抬升冷却史——低温年代学数据约束. 岩石学报, (4): 1167～1173.
李晨星, 常健, 邱楠生, 曹世纪, 张应鳞, 郑立庆. 2025. 原位 LA-ICP-MS 磷灰石裂变径迹实验流程建立与应用. 地球学报, 46(2): 471～482.
李瑞保, 裴先治, 刘战庆, 李佐臣, 丁仨平, 刘智刚, 张晓飞, 陈国超, 陈有炘, 王学良. 2010. 大巴山及川东北前陆盆地盆山物质耦合——来自 LA-ICP-MS 碎屑锆石 U-Pb 年代学证据. 地质学报, 84(8): 1118～1134.
李三忠, 张国伟, 周立宏, 赵国春, 刘鑫, 索艳慧, 刘博, 金宠, 戴黎明. 2011. 中、新生代超级汇聚背景下的陆内差异变形:华北伸展裂解和华南挤压逆冲. 地学前缘, 18(3): 79～107.
李双建, 孙冬胜, 蔡立国, 高平, 李天义, 袁玉松, 郑孟林, 邱登峰. 2018. 川北米仓山山前带碎屑锆石 U-Pb 年代学及盆山演化意义. 大地构造与成矿学, 42(6): 1087～1107.
李岩峰, 曲国胜, 刘殊, 张虹. 2008. 米仓山、南大巴山前缘构造特征及其形成机制. 大地构造与成矿学, (3): 285～292.
李永东, 熊熊, 冯雅杉. 2022. 南秦岭大巴山和米仓山-汉南穹隆中生代隆升幅度. 中国科学:地球科学, 52(03): 462～473.
林良彪, 陈洪德, 翟常博, 胡晓强, 李君文. 2006. 四川盆地西部须家河组砂岩组分及其古地理探讨. 石油实验地质, (06): 511～517.
刘祥, 詹琼窑, 朱弟成, 王青, 谢锦程, 张亮亮. 2021. 松潘-甘孜褶皱带南部上三叠统物源及构造抬升:碎屑锆石年代学和 Hf 同位素证据. 岩石学报, 37(11):3513～3538.
罗良, 漆家福, 张明正. 2015. 四川盆地周缘冲断带构造演化及变形差异性研究. 地质论评, 61(03): 525～535.
彭恒, 王建强, Massimiliano Z, 刘池洋, 韩鹏, 张少华. 2018. 晚三叠世-早侏罗世祁连山东部隆升的裂变径迹年代学证据及地质意义. 地球科学, 43(6): 1983～1996.
彭立勇. 2013. 米仓山-镇巴地区深部构造特征及其演化机制. 中国地质大学(北京)硕士学位论文.
邱楠生, 汪集暘, 梅庆华, 姜光, 陶成. 2010. (U-Th)/He 年龄约束下的塔里木盆地早古生代构造-热演化. 中国科学:地球科学, 40(12): 1669～1683.
邱楠生, 何丽娟, 常健, 朱传庆. 2020. 沉积盆地热历史重建研究进展与挑战. 石油实验地质, 42(5): 790～802.
孙东. 2012. 米仓山构造带构造特征及中-新生代构造演化. 成都理工大学博士学位论文.
田云涛, 朱传庆, 徐明, 饶松, Barry P K, 胡圣标. 2010. 白垩纪以来米仓山-汉南穹窿剥蚀过程及其构造意义:磷灰石裂变径迹的证据. 地球物理学报, 53(4): 920～930.
田云涛, 袁玉松, 胡圣标, 邱楠生. 2017. 低温热年代学在沉积盆地研究中的应用:以四川盆地北部为例. 地学前缘, 24(3): 105～115.
王启航. 2025. 四川盆地周缘中新生代定量变形重建. 中国地质大学(北京)硕士学位论文.
许军, 付强, 杨文涛. 2024. 华北盆地晚古生代碎屑锆石 U-Pb 年龄特征及其对周缘造山带的响应. 河南理工大学学报(自然科学版): 1～15.
闫心宇, 刘磊, 王小娟, 朱淑玥, 赵菲, 郑超, 马贤成, 张蕊. 2025. 川西北晚三叠世盆山耦合过程与古地理演化. 成都理工大学学报(自然科学版): 1～23.
闫义, 林舸, 王岳军, 郭锋. 2002. 盆地陆源碎屑沉积物对源区构造背景的指示意义. 地球科学进展: 85～90.
杨映涛, 付菊, 伍玲, 蒙欣. 2013. 川西坳陷中段上三叠统须家河组二、四段物源分析. 石油地质与工程, 27(6): 26～29＋148～149.
张国伟, 孟庆任, 赖绍聪. 1995. 秦岭造山带的结构构造. 中国科学(B辑), 38: 994～1003.
张国伟, 董云鹏, 赖绍聪, 郭安林, 孟庆任, 刘少峰, 程顺有, 姚安平, 张宗清, 裴先治, 李三忠. 2003. 秦岭-大别造山带南缘勉略构造带与勉略缝合带. 中国科学(D辑), 33(12): 1121～1135.
张国伟, 程顺有, 郭安林, 董云鹏, 赖绍聪, 姚安平. 2004. 秦岭-大别中央造山系南缘勉略古缝合带的再认识——兼论中国大陆主体的拼合. 地质通报, (Z2): 846～853.
张建勇, 常健, 李文正, 付小东, 杨磊, 和源. 2024. 川北米仓山隆起构造-热演化特征. 沉积与特提斯地质, 44(1): 58～70.
张茜. 2010. 米仓山隆升时代的沉积学制约. 西北大学硕士学位论文.
张文军, 秦绪乾, 郜瑭珺, 贺鸿冰. 2016. 米仓山隆起中新生代构造特征与形成演化探讨. 天然气技术与经济, 10(2): 22～25, 33, 82.
张勇. 2016. 四川盆地须家河组物源分析与扬子地块含油气岩层的重磁化研究. 南京大学博士学位论文.
朱晨曦. 2023. 米仓山-大巴山冲断带构造变形与演化研究. 中国石油大学(北京)硕士学位论文.

Multistage Mesozoic exhumation-erosion processes and tectono-sedimentary coupling in the southern margin of the Micang Mountain, South China

ZHANG Mengfei[1,2)], QIU Nansheng[*1,2)], CHANG Jian[*1,2)], FENG Qianqian[3)], LI Chenxing[1,2)], LIU Xin[1,2)], LONG Kangjie[1,2)]

1) *State Key Laboratory of Petroleum Resources and Engineering, China University of Petroleum, Beijing* 102249, *China*;

2) *College of Geosciences, China University of Petroleum, Beijing* 102249, *China*;

3) *College of Carbon Neutral Energy, China University of Petroleum, Beijing* 102249, *China*

* *Corresponding author*: *qiunsh@cup.edu.cn*; *changjian@cup.edu.cn*

Abstract

The formation of the Micang Mountain uplift is closely related to plate collision and the uplift of the Qinling orogenic belt. Previous research has predominantly focused on its uplift-erosion processes since the Middle-Late Mesozoic, though there remains controversy regarding its specific uplift process. This study selected Precambrian samples from the southern margin of the Micang Mountain uplift to conduct low-temperature thermochronology experiments, combined with detrital zircon U-Pb age data from Mesozoic strata in the region, to systematically reconstruct the multi-stage uplift-erosion history since the Early Mesozoic. The research results show that the median age range of zircon fission tracks is 277±27 Ma to 399±39 Ma, while the zircon (U-Th)/He age range is 136.4±6.8 Ma to 290.0±14.5 Ma. Through thermal history simulation, the tectonic evolution of the Micang Mountain uplift since the Mesozoic can be divided into four stages: ① from the Late Triassic to the Middle Jurassic, affected by the closure of the Mianlue Ocean and the subduction of the Yangtze Block under the Qinling block, the Micang Mountain region began an initial slow uplift; ② from the Late Jurassic to the Early Cretaceous, the continuous collision between the Qinling block and the Yangtze Block triggered intense intracontinental orogeny, leading to rapid uplift of the Micang Mountain region; ③ from the Late Cretaceous to the Neogene Miocene, the region entered a brief tectonic quiescence period due to adjustments in regional plate movements; ④ since the Miocene, affected by the eastward propagation of the Tibetan Plateau's uplift, the region has experienced another phase of rapid uplift and denudation. Detrital zircon U-Pb age spectra indicate a significant increase in Neoproterozoic zircons in the strata from the Upper Triassic to the Lower Jurassic, indicating that uplift had already initiated in the Late Triassic, which aligns well with the initial uplift timing indicated by low-temperature thermochronology data. This study reconstructs the tectono-thermal evolutionary history of the southern margin of the Micang Mountain uplift since the Mesozoic, clarifies the temporal and spatial coupling relationship between the multi-stage uplift-erosion processes and multi-episodic plate tectonic movements, and provides new evidence for understanding plate collision dynamics and Qinling Orogen evolution.

Key words: Micang Mountain; tectono-thermal evolution; low-temperature thermochronology; Mesozoic; provenance analysis